Thieno[3,4-*d*]pyrimidin-4(1H)-thione: An Effective, Oxygenation Independent, Heavy-Atom-Free Photosensitizer for Cancer Cells

Luis A. Ortiz-Rodríguez,[1] Ye-Guang Fang,[2] Germain Niogret,[2] Kaivin Hadidi,[3] Sean J. Hoehn,[1] Heather J. Folkwein,[1] Steffen Jockusch,[4] Yitzhak Tor,[3,*] Ganglong Cui,[2,*] Liraz Levi,[5,6*] Carlos E. Crespo-Hernández[1,*]

[1] Department of Chemistry, Case Western Reserve University, Cleveland, OH, USA 44106
[2] Key Lab of Theoretical and Computational Photochemistry, Ministry of Education, Chemistry College, Beijing Normal University, Beijing, 100875, China
[3] Department of Chemistry and Biochemistry, University of California, San Diego, La Jolla, CA, USA 92093
[4] Center for Photochemical Sciences, Bowling Green State University, Bowling Green, Ohio, USA 43403
[5] Celloram Inc, Cleveland, OH, USA 44106
[6] Department of Pediatrics, Case Western Reserve University School of Medicine, Cleveland, Ohio USA 44106

Supporting Information

S1. Methods

S1.1 Materials and Steady-State Measurements

The synthesis, as well as analytical (mass spectrometry, ^{1}H and ^{13}C-NMR) and crystal structure data for ThiaHX and ThiathioHX (structures in Scheme 1) are provided in the SI. Phosphate buffer was freshly prepared using 0.2996 (± 0.0001) g of monobasic sodium phosphate and 0.2314 (± 0.0001) g of dibasic sodium phosphate dissolved in 250 mL of ultrapure water and adjusted to pH 7.4 using a concentrated sodium hydroxide (NaOH) solution, with a total phosphate concentration of 16 mM. Phosphate salts and NaOH were purchased from Fisher Scientific, Inc. Acetonitrile (MeCN) was purchased from Fisher Scientific, Inc. Calf thymus DNA (Sigma-Aldrich) was used as received. Steady-state absorption and emission spectroscopy were performed using a Cary 300 and Cary Eclipse spectrometers, respectively. Fluorescence spectra were taken at PMT voltage of 800 V for ThiathioHX in phosphate buffer pH 7.4 and MeCN, 600 V for ThiaHX in MeCN and 400 V for ThiaHX in phosphate buffer pH 7.4 with slit widths of 5 nm. Relative fluorescence quantum yields were obtained by using the riboside of 2-aminopurine as standard for both solvents (ϕ_F = 0.26 and 0.68 in MeCN and phosphate buffer, respectively).[1]

S1.2 Broadband femtosecond transient absorption spectroscopy

Femtosecond transient absorption spectroscopy (fs-TAS) was used to study the excited-state dynamics of ThiaHX and ThiathioHX. The setup is described in detail in previous publications.[2,1,3] Briefly, a Ti:Spapphire oscillator (Vitesse, Coherent, Santa Clara, CA, USA) seed a regenerative amplifier (Coherent Libra-HE) that generates 100 fs pulses at 800 nm with a repetition rate of 1 kHz is used to pump a Traveling Optical

Parametric Amplifier of Superfluorescence (TOPAS, Quantronix/Light Conversion, Vilnius, Lithuania). In this work, the TOPAS was tuned to 325 and 385 nm. A translating 2 mm CaF_2 crystal was used to generate the white light continuum for probing (ca. 320 to 700 nm). The setup employs a mechanical delay stage with a physical temporal limit of 3 ns. The excitation pulses were set to a power of 1.75 mW (measured at the optical cell position) using a neutral density filter. A 2 mm optical cell was used. The solution was continuously stirred with a Teflon-coated magnetic stirrer. All solutions were kept below 10% degradation, as judged from the absorption spectra taken at 308 and 367 nm before and after irradiation with the laser for ThiaHX and ThiathioHX, respectively. Data analysis made use of Glotaran software package.[4] The fs-TAS data were fit to a two-component sequential kinetic model.

S1.3 Laser flash photolysis

Laser flash photolysis experiments were used to characterize the triplet state of ThiaHX and ThiathioHX. These experiments employed pulses generated by a Lambda Physik COMPex Excimer laser with excitation wavelengths of 308 nm (ThiaHX) and a Spectra Physics GCR-150-30 Nd:YAG laser with excitation wavelengths of 355 nm (ThiathioHX) and a computer controlled system that has been described in detail elsewhere.[5] Experiments were performed in a 1 cm optical cell with an absorbance at the excitation wavelength of ~0.3 in phosphate buffer at pH 7.4 and MeCN. Deoxygenated solutions were prepared by purging with ultrapure argon gas for at least 20 minutes.

S1.4 Singlet oxygen quantum yields

Nanosecond time-resolved luminescence spectroscopy was used to determine the singlet oxygen quantum yields for ThiaHX and ThiathioHX. Briefly, a COMPex Excimer

laser (Lambda Physik, 308 nm, 20 ns pulse width) and a GCR-150-30 Nd:YAG laser (Spectra Physics, 355 nm, 7 ns pulse width) was used as the excitation source. An excitation wavelength of 308 and 355 nm was used for ThiaHX and ThiathioHX, respectively. Singlet oxygen phosphorescent decay traces were collected at 1270 nm using a modified Fluorolog-3 spectrometer (HORIBA, Jobin Yvon), with a near-IR sensitive photomultiplier tube (H10330A-45, Hamamatsu) as detector. The decay traces were stored on a digital oscilloscope (TDS 360, Tektronics). Solutions of ThiaHX, ThiathioHX and the phenalenone standard were prepared in Tris-buffered D_2O and acetonitrile at an optical density of 0.3 at 308 nm (ThiaHX) and 355 nm (ThiathioHX) in 1 cm path length quartz cuvettes. The O_2-saturated solutions were bubbled with ultrapure oxygen gas for at least 20 min prior to testing. Degradation of the samples was determined to be less than 3% over the course of the experiments based on their steady-state absorption spectra. The quantum yields were determined in back-to-back luminescence experiments of ThiaHX, ThiathioHX and phenalenone solutions under the same conditions, using the reported yield of $^1O_2$ generated by phenalenone as a standard ($\phi_\Delta = 0.98$).[6]

S1.5 Cell culture and treatment with ThiathioHX

Human cervical adenocarcinoma (HeLa) and mouse melanoma (BF16F10) cell lines were incubated in complete medium (Dulbecco's modified Eagle's Medium, DMEM) and were seeded at 2000 cells/well in a 96-well plate and allowed to adhere for 24 hours. Following the 24 hours, the cells were treated and incubated for two hours with ThiathioHX using dimethylsulfoxide as a vehicle. Seven different concentrations (4 to 166 μM) of ThiathioHX were used. Prior to irradiation, the cells were washed three times with phosphate-buffered saline solution (PBS) and then fresh medium was added. Cells were irradiated with 5 J cm^{-2} of UVA light (350 to 410 nm,

λ_{max} = 370 nm) through the clear polystyrene bottom of the 96-well plate (see the transmittance spectrum in Figure S20a). The lamp intensity was measured at the position of cell growth (the bottom of the wells) using a ThorLabs photodiode (S120VC). The reflection, scattering and absorption by the polystyrene bottom were considered by measuring the lamp intensity through a polystyrene filter of the same thickness. The lamp spectrum was collected through the same polystyrene filter using a fiber optic spectrometer (lamp spectrum is reported in Figure S20b). After irradiation, cells were incubated for 24 hours after which cell viability was determined using the PrestoBlue (Invitrogen) assay.[7,8] PrestoBlue's fluorescence (λ_{exc} = 560 nm/λ_{em} = 590 nm) was measured using a Spectra Max i3X (Molecular Devices) and quantified with the SoftMax Pro 6 software. Results reported are the mean of 3 replicates and the errors correspond to the standard deviation. A similar methodology to the one described above was followed for the experiments performed under hypoxic (5% oxygen) conditions, with the only two exceptions being that the incubation with ThiathioHX for two hours and the UVA (5 J cm^{-2}) treatment was done in an incubator with an atmosphere of 5% oxygen, 5% carbon dioxide and 90% nitrogen.

S1.6 Live-dead cell staining

BF16F10 and HeLa cells were seeded at 20000 cells/well in a 6-well plate and allowed to adhere for 24 hours. Following the 24 hours, the cells were treated and incubated with ThiathioHX (125 μM) using dimethylsulfoxide as a vehicle. Prior to irradiation, the cells were washed three times with PBS and then fresh medium was added. Cells were irradiated with 5 J cm^{-2} of UVA light (350 to 410 nm, λ_{max} = 370 nm) through the clear polystyrene bottom of the 6-well plates. For the cells under hypoxic conditions, the same methodology was followed, but under 5% oxygen conditions. After treatment, the cells were incubated for 1.5 hours and subsequently fixed with 4% paraformaldehyde. Following

fixing, the cells were stained with 4′,6-diamidino-2-phenylindole (DAPI, 1 μg/mL), propidium iodide (PI, 0.5 μg/mL) and Annexin V-Alexa Fluor™ 488 (Annexin V, 0.25 μg/mL).[9–11] The cells were imaged with a Keyence BZ-X810 fluorescence microscope. An exposure time of 1/2.5 s and a 10X lens were used in all measurements. The blue, green, and red channels were used to measure the fluorescence of DAPI, Annexin V and PI, respectively.

S1.7 Detection and qualification of ROS in vitro

BF16F10 and HeLa cells were incubated in Fluorobrite DMEM and were seeded at 2000 cells/well in a 96-well plate and allowed to adhere for 24 hours. Following the 24 hours, the cells were treated and incubated for 2 hours with ThiathioHX, using dimethylsulfoxide as a vehicle. Seven different concentrations (4 to 166 μM) of ThiathioHX were used. After incubation with ThiathioHX the medium was replaced by fresh medium containing 10 μM of the reactive oxygen species reporter 2,7-dichlorohydrofluorescein diacetate (DCF-DA, >95% purity, Cayman Chemical Company). Cells were incubated with the DCF-DA medium for 30 minutes. The medium was then removed, the cells were rinsed three times with PBS and then fresh Fluorobrite DMEM medium was added. The fluorescence intensity at 488 nm of DCF-DA was measured using a Spectra Max i3X (Molecular Devices) and quantified with the SoftMax Pro 6 software.[12] For the cells under hypoxic conditions, the same methodology was followed, but under a 5% oxygen conditions.

S1.8 Computational methods

Minimum-energy structures, conical intersections, and crossing points of ThiaHX and ThiathioHX in the electronically excited and ground states were directly optimized by

the complete active space second order perturbation theory (CASPT2) method[13,14] using the free OpenMolcas package.[15,16] In the geometry optimization, the cc-pVDZ basis sets[17] were used for all atoms without geometry constraints. The further single-point energy refinement of all the optimized structures was carried out with a larger aug-cc-pVTZ basis set,[17] explicit solvent molecule (acetonitrile and water) together with the implicit polarizable continuum model (PCM)[18,64] are used to consider the solvation effects. In all the CASPT2 calculations, an active space of 12 electrons in 10 orbitals was used. The Cholesky decomposition technique[19] for approximating two-electron integrals was employed; the electron ionization affinity (IPEA) shift[20] was set to zero and the imaginary shift technique (0.2 a.u.)[21] was carried out to avoid the issue of the intruder state. Spin-orbit coupling (SOC) constants are calculated at the CASPT2/aug-cc-pVTZ level of theory under the atomic mean-field approximation (AMFI), the effective spin-orbit coupling $\langle \boldsymbol{\Psi_I} | \boldsymbol{H_{eff}^{so}} | \boldsymbol{\Psi_J} \rangle$ is calculated by using the following equation (1):

$$\langle \boldsymbol{\Psi_I} | \boldsymbol{H_{eff}^{so}} | \boldsymbol{\Psi_J} \rangle = \sqrt{\frac{(\langle \boldsymbol{\Psi_I} | \boldsymbol{H_x^{so}} | \boldsymbol{\Psi_J} \rangle)^2 + (\langle \boldsymbol{\Psi_I} | \boldsymbol{H_y^{so}} | \boldsymbol{\Psi_J} \rangle)^2 + (\langle \boldsymbol{\Psi_I} | \boldsymbol{H_z^{so}} | \boldsymbol{\Psi_J} \rangle)^2}{3}} \quad (1)$$

in which $\boldsymbol{\Psi_I}$ and $\boldsymbol{\Psi_J}$ represent singlet and triplet states wavefunctions, $\boldsymbol{H_x^{so}}$, $\boldsymbol{H_y^{so}}$, and $\boldsymbol{H_z^{so}}$ are x, y, and z components of spin-orbit operators. To verify the effects of the relativistic basis set on the SOC interaction of ThiaHX and ThiathioHX, the relativistically contracted atomic natural orbital basis sets ANO-RCC-VTZP are employed to calculate the SOCs (in cm^{-1}). As shown in Table S6, the relativistic basis sets give nearly same results. Finally, the crossing point structures are determined by the projected constrained optimization method.[22] All SOC values and crossing-point structures are obtained using the OpenMolcas package.[15,16] The excited state

absorption spectra were calculated using the same level of theory as that used in the single point refinements.

S2. Supporting Experimental and Computational Results and Discussion

S2.1 Steady state absorption and emission

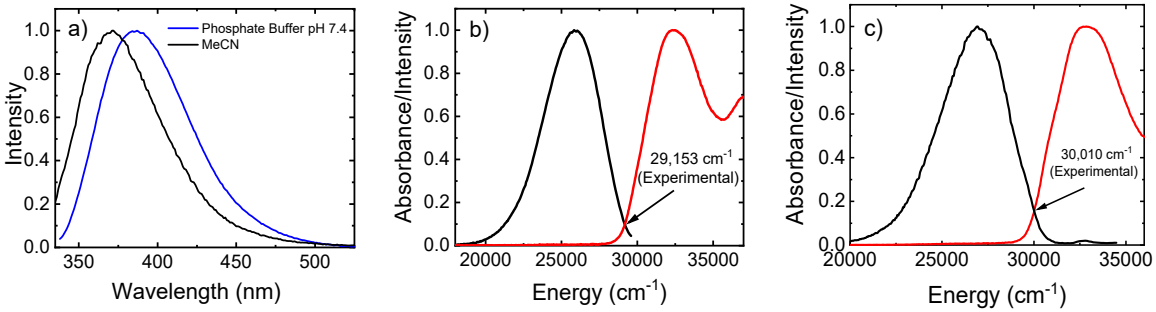

Figure S1. (a) Normalized emission spectra of ThiaHX in phosphate buffer pH 7.4 and in MeCN. Collection of the emission spectra of ThiathioHX in each solvent was attempted but no emission signal was detected. (b) Emission spectrum overlaid with absorption spectrum of ThiaHX in phosphate buffer at pH 7.4 to obtain the E_{00}. (c) Emission spectrum overlaid with absorption spectrum of ThiaHX in acetonitrile to obtain the E_{00}. E_{00} energies of 29,153 cm^{-1} (3.61 eV) and of 30,010 cm^{-1} (3.72 eV) were obtained from the crossing point of the normalized absorption and emission spectra of ThiaHX in phosphate buffer and in MeCN, respectively.

S2.2 Theoretical results

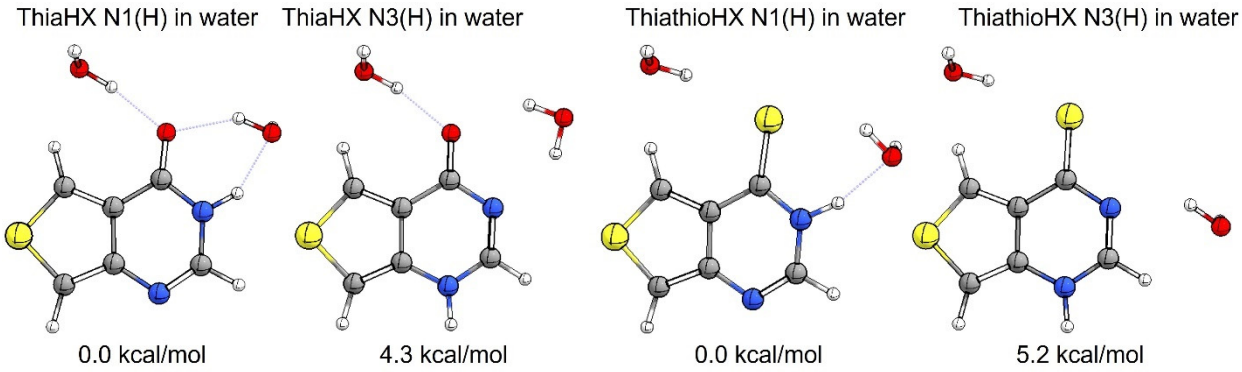

Figure S2. Ground-state optimized structures in water at the CASPT2(12,10)/cc-pVDZ level of theory. Relative energies were obtained at the CASPT2(12,10)/aug-cc-pVTZ level of theory.

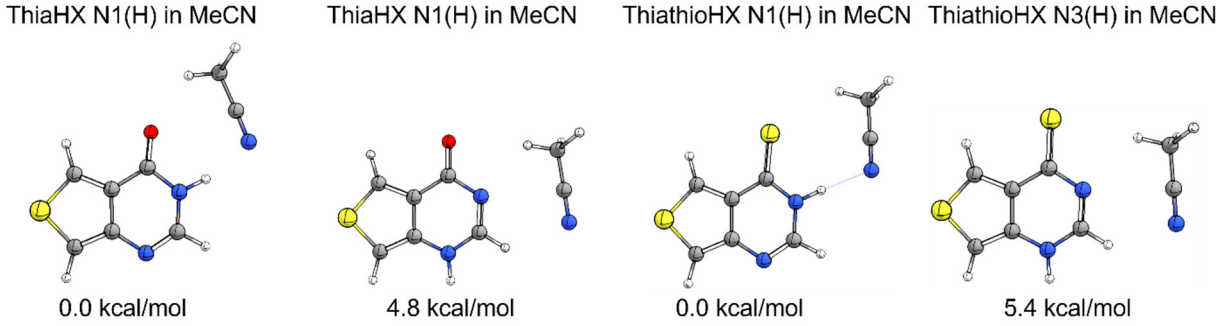

Figure S3. Ground-state optimized structures in MeCN at the CASPT2(12,10)/cc-pVDZ level of theory. Relative energies were obtained at the CASPT2(12,10)/aug-cc-pVTZ level of theory.

Based on the molecular structures of ThiaHX and ThiathioHX, two possible tautomers can be expected to be available in solution. As mentioned in the paper, quantum chemical calculations at the CASPT2 level of theory in water and acetonitrile suggest that the N1(H) tautomer is >4 and >5 kcal mol^{-1} more stable than the N3(H) tautomer in ThiaHX and ThiathioHX, independently of the solvent. These results agree with the recent work of Sholokh et al.,[1] where they show that the N1(H) tautomer is the most stable in solution for thienoguanosine at the PBE0/PCM and M052X/PCM level of theories.[23]

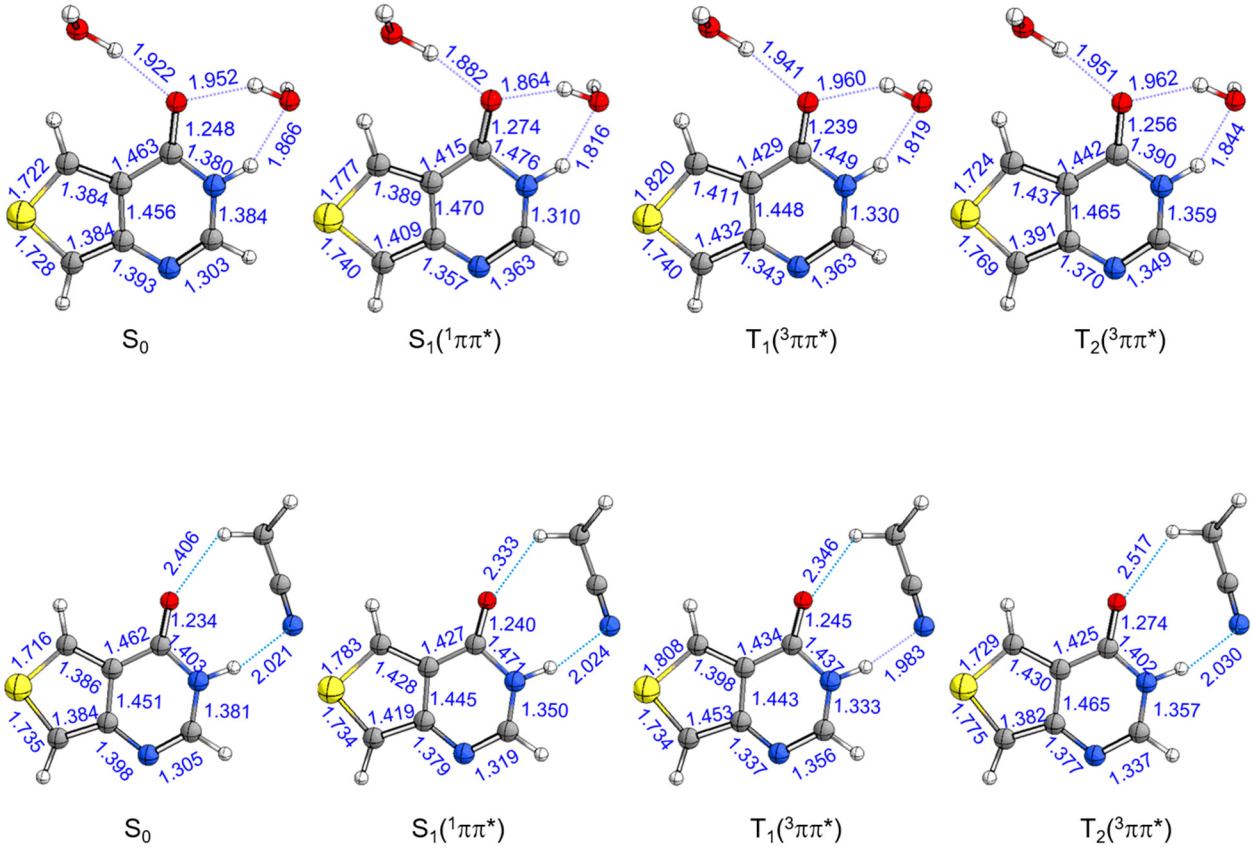

Figure S4. Minima structures of ThiaHX optimized at the CASPT2/cc-PVDZ level of theory in water (top) and MeCN (bottom). Selected bond lengths are given in angstroms.

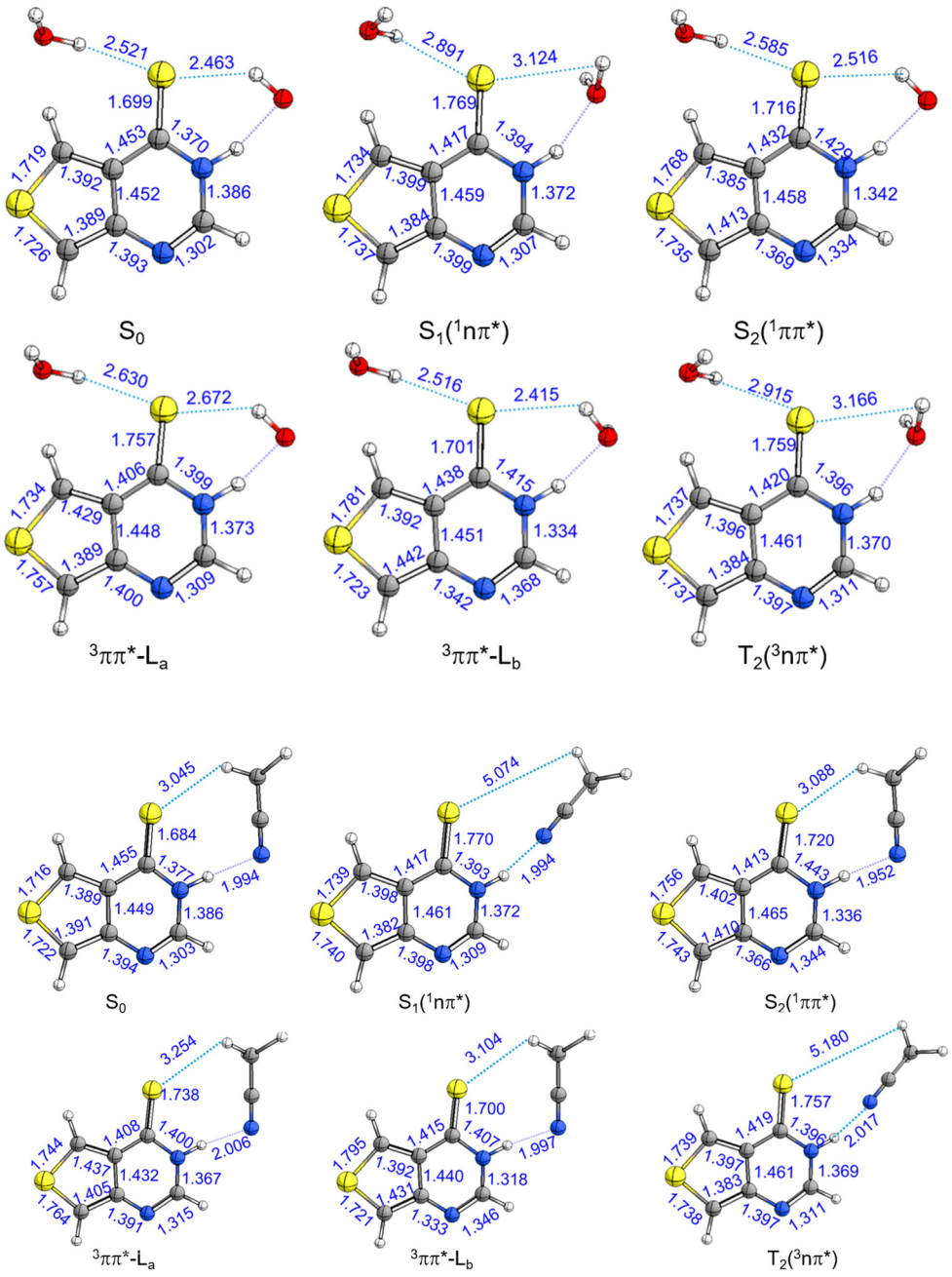

Figure S5. Minima structures of ThiathioHX optimized at the CASPT2/cc-PVDZ level of theory in water (top) and MeCN (bottom). Selected bond lengths are given in angstroms.

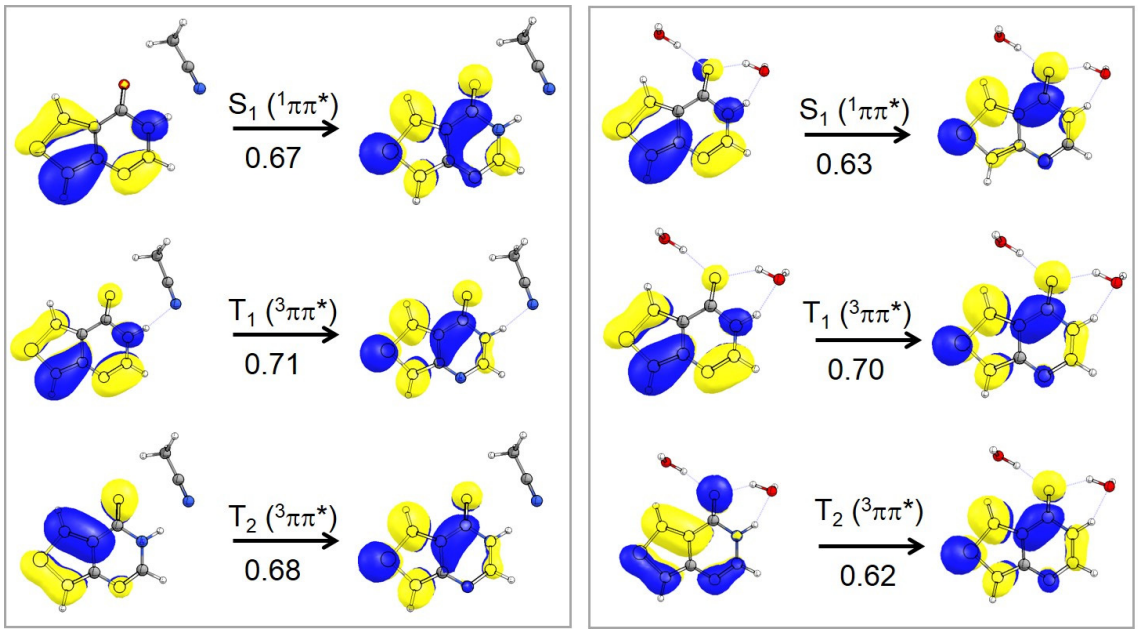

Figure S6. CASPT2 computed main electronic configurations at the corresponding minima of ThiaHX in MeCN (left) and water (right), respectively.

Table S1. Vertical excitation energies for ThiaHX in MeCN obtained at the CASPT2(12,10)/aug-cc-pVTZ/PCM level of theory.

	Energies (kcal/mol)	Osc. Strength (*f*)	Configurations	Weights
$S_1(^1\pi\pi^*)$	88.0	0.21	2222u2d000 22222ud000	0.34897 0.22041
$S_2(^1\pi\pi^*)$	93.1	0.03	2222u2d000 22222ud000	0.37827 0.17819
$T_1(^3\pi\pi^*)$	69.4	0.00	2222u2u000 22222uu000	0.51491 0.23734
$T_2(^3\pi\pi^*)$	86.1	0.00	22222uu000 2222u200u0	0.40599 0.31228

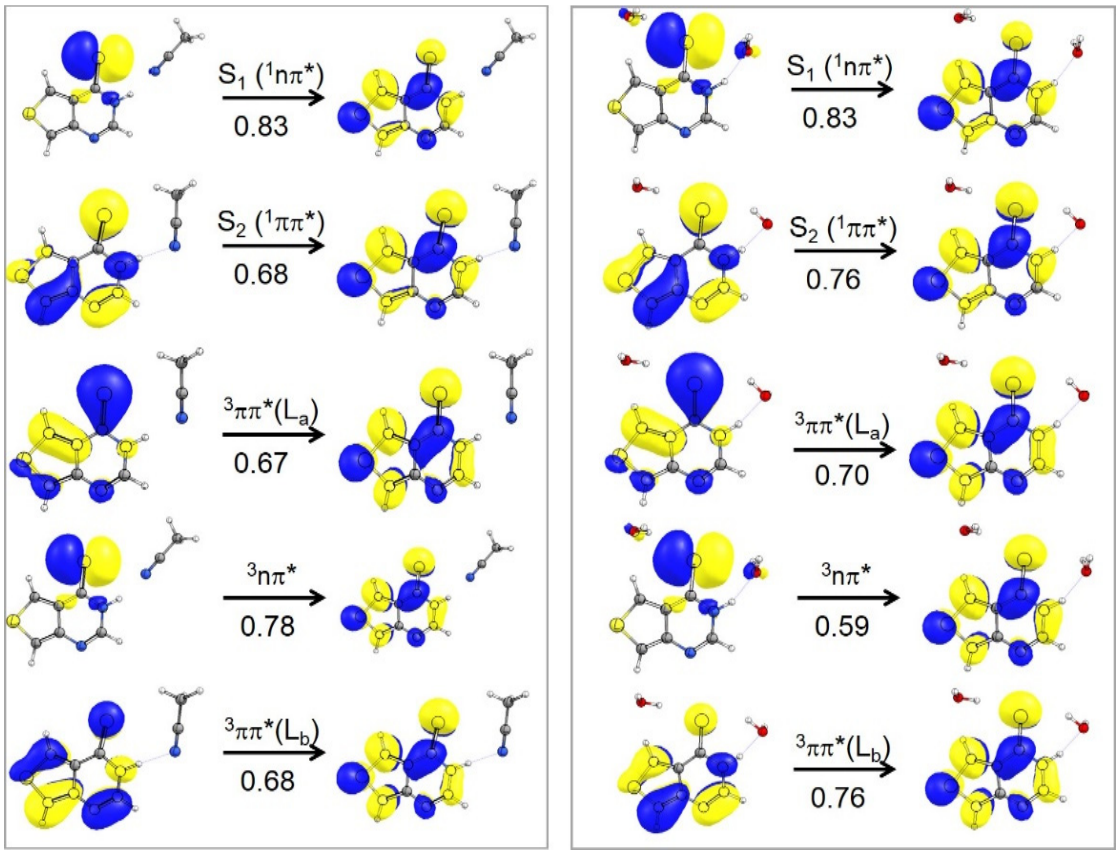

Figure S7. CASPT2 computed main electronic configurations at the corresponding minima of ThiathioHX in MeCN (left) and water (right), respectively.

Table S2. Vertical excitation energies for ThiathioHX in MeCN obtained at the CASPT2(12,10)/aug-cc-pVTZ level of theory.

	Energies (kcal/mol)	Osc. Strength (*f*)	Configurations	Weights
$S_1(^1n\pi^*)$	61.6	1.9×10^{-5}	22222ud000	0.82840
$S_2(^1\pi\pi^*)$	71.4	0.45	2222u2d000	0.68156
$(^3\pi\pi^*)$-L_a	57.6	0.0	2u2222u000 2222u2u000	0.40108 0.38230
$^3n\pi^*$	58.3	0.0	22222uu000	0.76535
$(^3\pi\pi^*)$-L_b	63.6	0.0	2222u2u000 2u2222000u	0.29178 0.18296

Table S3. CASPT2(12,10)/aug-cc-pVTZ calculated adiabatic excitation energies (in eV) of ThiaHX in water and acetonitrile.

	$S_1(^1\pi\pi^*)$	$T_1(^3\pi\pi^*)$	$T_2(^3\pi\pi^*)$	S_1/S_0
water	3.53	2.37	3.43	4.19/3.46 (avoided CI)
MeCN	3.56	2.55	3.55	5.12/4.56 (avoided CI)

Table S4. CASPT2(12,10)/aug-cc-pVTZ calculated adiabatic excitation energies (in eV) of ThiathioHX in water and acetonitrile.

	$S_1(^1n\pi^*)$	$S_2(^1\pi\pi^*)$	S_2/S_1	S_1/S_0	$^3\pi\pi^*$-L_a	$^3\pi\pi^*$-L_b	$^3n\pi^*$
water	2.48	2.87	2.89/2.86	3.03/2.99	2.42	2.48	2.32
MeCN	2.47	2.85	2.89/2.88	3.22/3.06	2.37	2.41	2.27

Table S6. Spin-orbit coupling (SOC) constants (in cm^{-1}) calculated at the CASPT2/ANO-RCC-VTZP/PCM (acetonitrile) and CASPT2/aug-cc-pVTZ/PCM (acetonitrile) levels for ThiaHX and ThiathioHX.

	ThiaHX	ThiathioHX	
	SOC (S_1/T_2)	SOC ($^1n\pi^*/^3\pi\pi^*$-L_a)	SOC ($^1n\pi^*/^3n\pi^*$)
ANO-RCC-VTZP	0.38	90.75	6.76
cc-pVTZ	0.06	93.34	5.79

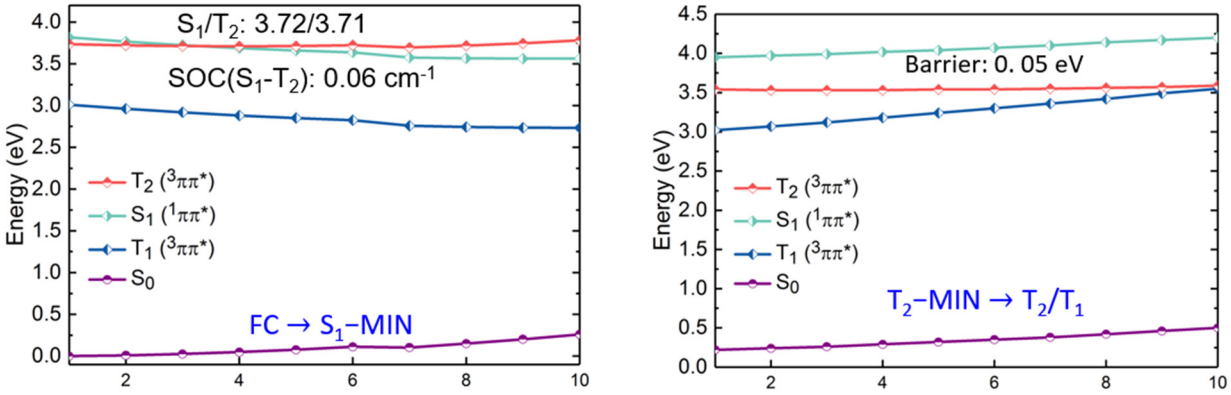

Figure S8. CASPT2(12,10)/aug-cc-pVTZ (MeCN) calculated ThiaHX linearly interpolated internal coordinate (LIIC) paths connecting the Franck-Condon point and the S_1 minimum and the T_2-minimum with the T_2/T_1 crossing point.

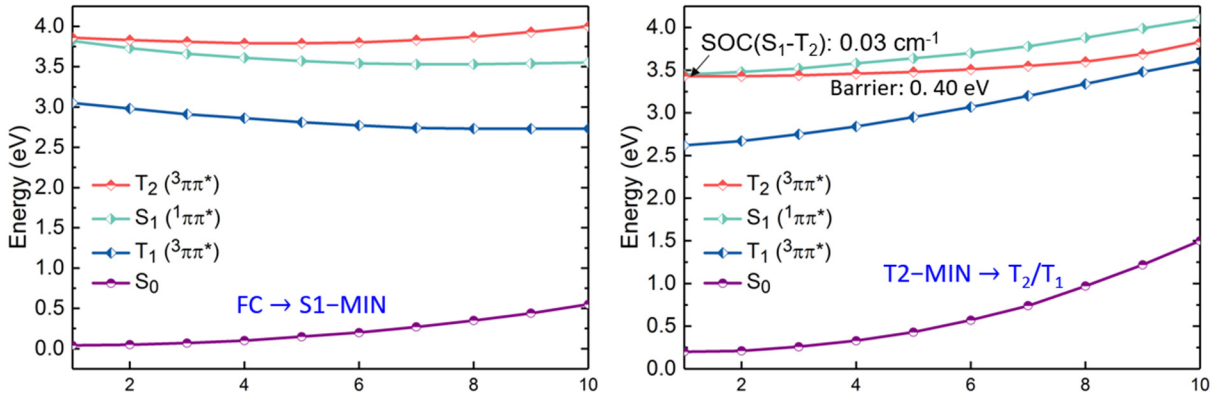

Figure S9. CASPT2(12,10)/aug-cc-pVTZ (water) calculated ThiaHX linearly interpolated internal coordinate (LIIC) paths connecting the Franck-Condon point and the S_1 minimum and the T_2-minimum with the T_2/T_1 crossing point.

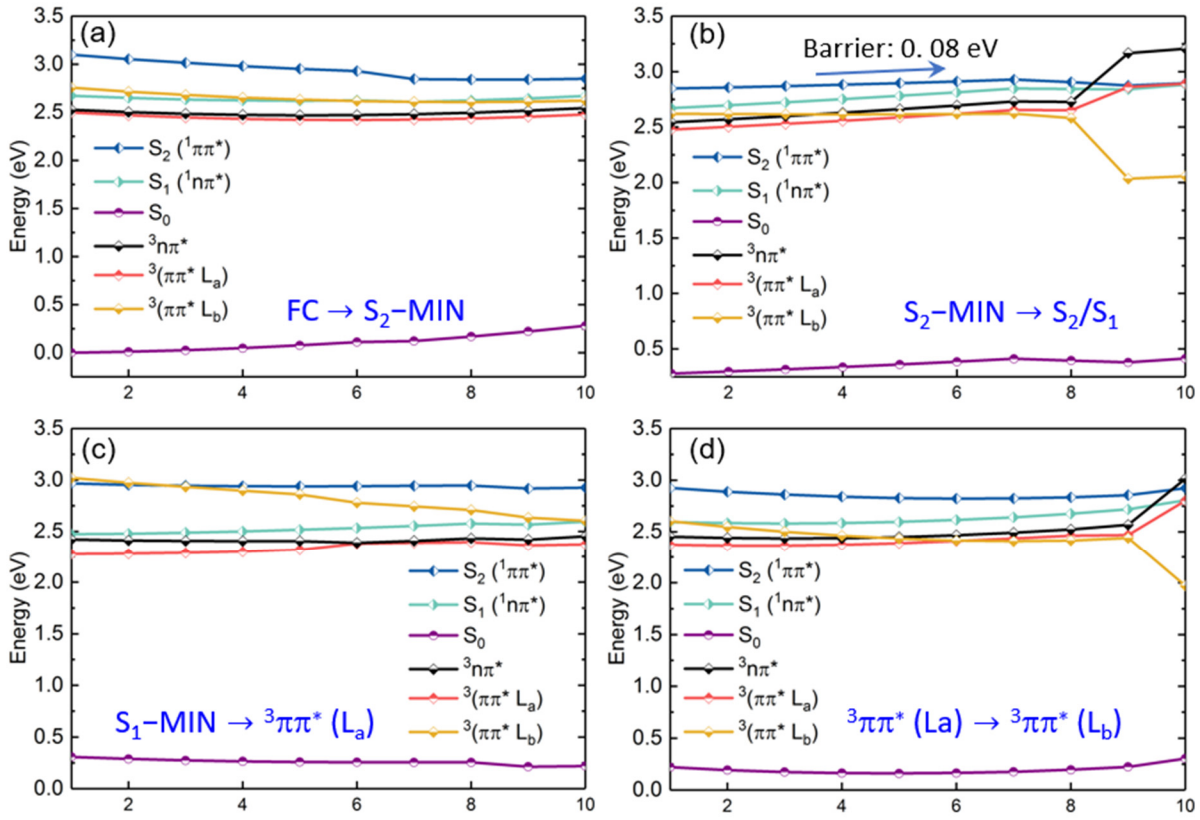

Figure S10. CASPT2(12,10)/aug-cc-pVTZ (MeCN) calculated ThiathioHX linearly interpolated internal coordinate (LIIC) paths connecting (a) the Franck-Condon point and S_2 minimum; (b) the S_2 minimum and S_2/S_1 conical intersection; (c) the S_1 minimum and $^3\pi\pi^*(L_a)$ minimum; (d) the $^3\pi\pi^*(L_a)$ minimum and $^3\pi\pi^*(L_b)$ minimum.

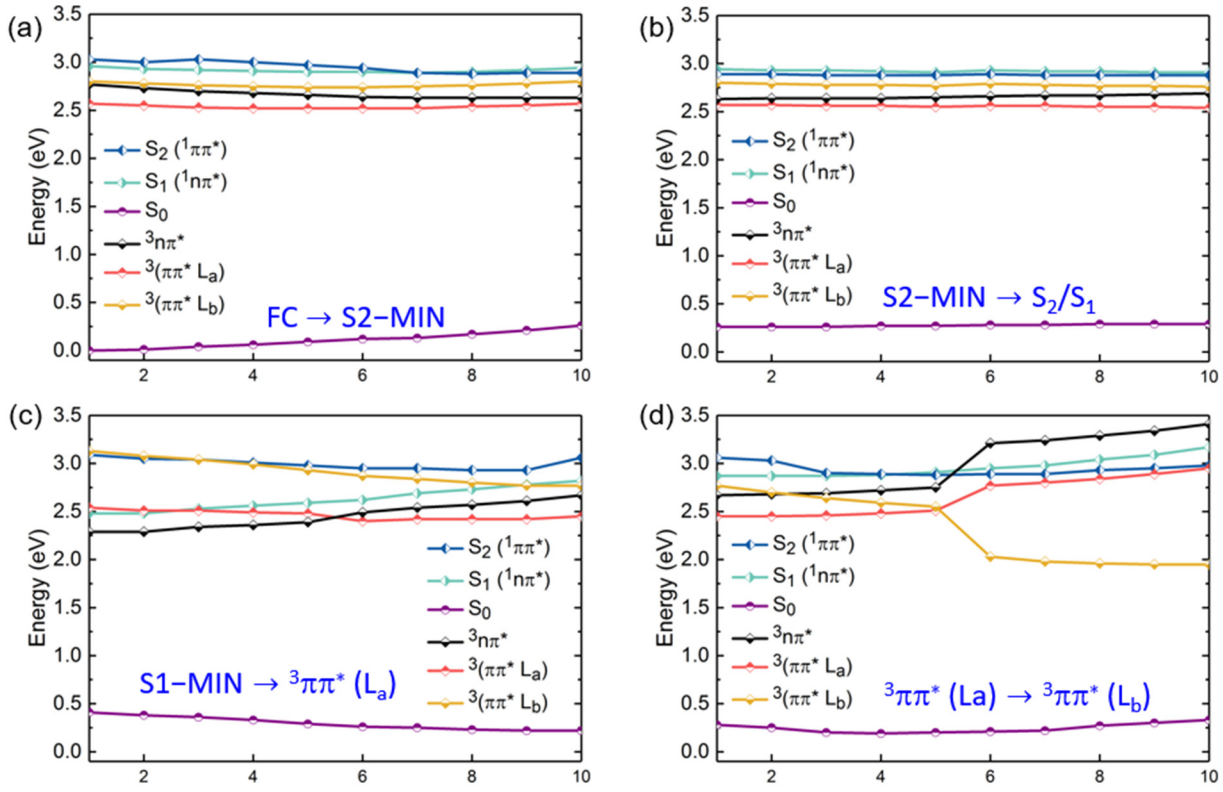

Figure S11. CASPT2(12,10)/aug-cc-pVTZ (water) calculated ThiathioHX linearly interpolated internal coordinate (LIIC) paths connecting (a) the Franck-Condon point and S_2 minimum; (b) the S_2 minimum and S_2/S_1 conical intersection; (c) the S_1 minimum and $^3\pi\pi^*(L_a)$ minimum; (d) the $^3\pi\pi^*(L_a)$ minimum and $^3\pi\pi^*(L_b)$ minimum.

Upon excitation to its $^1\pi\pi^*$ state in the Franck-Condon region (3.82 eV), ThiaHX is expected to rapidly relax to its excited state minimum, where it can access a $^1\pi\pi^*/S_0$ conical intersection and/or a $^1\pi\pi^*/T_2(^3\pi\pi^*)$ crossing region. However, the $^1\pi\pi^*/S_0$ conical intersection is more than 0.6 eV higher in energy than the $^1\pi\pi^*$ minimum in both solvents and thus, internal conversion to the ground state is not a major deactivation pathway for ThiaHX. Although the $^1\pi\pi^*/T_2(^3\pi\pi^*)$ crossing region can be accessed barrierlessly from the $^1\pi\pi^*$ minimum, the corresponding spin-orbit coupling (SOC) is expected to be small due to the $\pi\pi^*$ character of both excited states, as predicted by the well-known El-Sayed rule. [71,72] This is further supported by the

calculated SOC values of 0.03 and 0.06 cm^{-1} at the $^1\pi\pi^*/T_2(^3\pi\pi^*)$ crossing point (CASPT2(12,10)/aug-cc-pVTZ) in water and MeCN, respectively.

In MeCN, the potential energy surfaces of the $^1\pi\pi^*$ and $T_2(^3\pi\pi^*)$ states are essentially isoenergetic throughout, as illustrated in the FC→$^1\pi\pi^*$ minimum LIIC paths (Figures S13 and S14). This, in combination with the stronger SOC in the crossing region, suggests that $^1\pi\pi^*/T_2(^3\pi\pi^*)$ intersystem crossing should occur more rapidly in MeCN than in aqueous solution. If the $T_2(^3\pi\pi^*)$ state is populated, it will decay to the lower $T_1(^3\pi\pi^*)$ state via the T_2/T_1 conical intersection. This process needs to overcome a barrier of 0.05 and 0.4 eV in MeCN and water, respectively. Hence, T_2/T_1 internal conversion is expected to occur faster in MeCN. In the $T_1(^3\pi\pi^*)$ state, the population is predicted to stay for a relatively long time because there is a large energy barrier separating the $T_1(^3\pi\pi\ ^*)$ minimum and the $T_1(^3\pi\pi\ ^*)/S_0$ crossing point and hence, increasing the probability of photochemical and/or photosensitization reactions. The energy barrier is calculated to be 0.51 and 0.47 eV relative to the T_1 minimum in MeCN and water, respectively.

Conversely, according to the calculated vertical excitation energies for ThiathioHX, excitation at 325 nm directly populates the $^1\pi\pi^*$ state at the Franck-Condon region (3.10 eV). Then, it is predicted to relax smoothly to its minimum, releasing ~0.2 eV energy in the $^1\pi\pi^*$ state in both solvents. Importantly, near the $^1\pi\pi^*$ minimum, there is an isoenergetic $^1\pi\pi^*/^1n\pi^*$ conical intersection (see Figure 6b). Hence, the $^1\pi\pi^*\rightarrow\ ^1n\pi^*$ internal conversion process is predicted to occur efficiently and should be a major excited-state relaxation pathway for the population reaching the $^1\pi\pi^*$ state. In addition to the $^1\pi\pi^* \rightarrow\ ^1n\pi^*$ internal conversion process, the $^1\pi\pi^* \rightarrow\ ^3n\pi^*$ intersystem crossing pathway could play a role in the excited-state decay of the $^1\pi\pi^*$ state because the SOC value at this crossing point is

relatively large (i.e., 54.7 cm^{-1}) and the crossing region is only 0.08 eV higher in energy than the $^1\pi\pi^*$ minimum. However, due to the presence of the small energetic barrier, $^1\pi\pi^* \rightarrow {}^1n\pi^*$ internal conversion is predicted to dominate as a deactivation pathway over $^1\pi\pi^* \rightarrow {}^3n\pi^*$ intersystem crossing. Furthermore, internal conversion from the $^1n\pi^*$ state to the ground state is not expected to be a relevant relaxation pathway because the $^1n\pi^*/S_0$ conical intersection is ~0.6 eV above the $^1n\pi^*$ minimum. The $^1n\pi^* \rightarrow {}^3n\pi^*$ intersystem crossing is not expected to be favorable considering the El-Sayed rules[71,72] because both excited states have $n\pi^*$ character and the corresponding SOC value is estimated to be 5.79 cm^{-1} at the CASPT2(12,10)/aug-cc-pVTZ level. Instead, intersystem crossing from $^1n\pi^* \rightarrow {}^3\pi\pi^*$-$L_a$ following the internal conversion event is expected to play a major role. The crossing region can be accessed in a barrierless fashion and the SOC at the crossing point is relative strong 83.3 cm^{-1}. Hence, we expect $^1n\pi^* \rightarrow {}^3\pi\pi^*$-$L_a$ to be the primary intersystem crossing pathway.

According to the CASPT2(12,10)/aug-cc-pVTZ calculations, there are two main nonradiative excited-state relaxation pathways that could occur from the $^3\pi\pi^*$-L_a state. In the first one, the system can evolve from the $^3\pi\pi^*$-L_a state into the energetically lower $^3\pi\pi^*$-L_b state because it can be accessed in a barrierless fashion at the CASPT2(12,10)/aug-cc-pVTZ level of theory (see Figures S15d and S16d). In the second pathway, the system can decay to the S_0 state through the $T_1 \rightarrow S_0$ intersystem crossing process because the $^3\pi\pi^*$- L_a potential energy surface can cross the ground state at a $^3\pi\pi^*$- L_a/S_0 crossing region. Nonetheless, the latter process needs to surmount an energy barrier of ~0.7 eV. Overall, the evolution into the significantly more stable $^3\pi\pi^*$-L_b state should be preferred outcome in both solvents.

S2.3 Calculated excited state absorption spectra

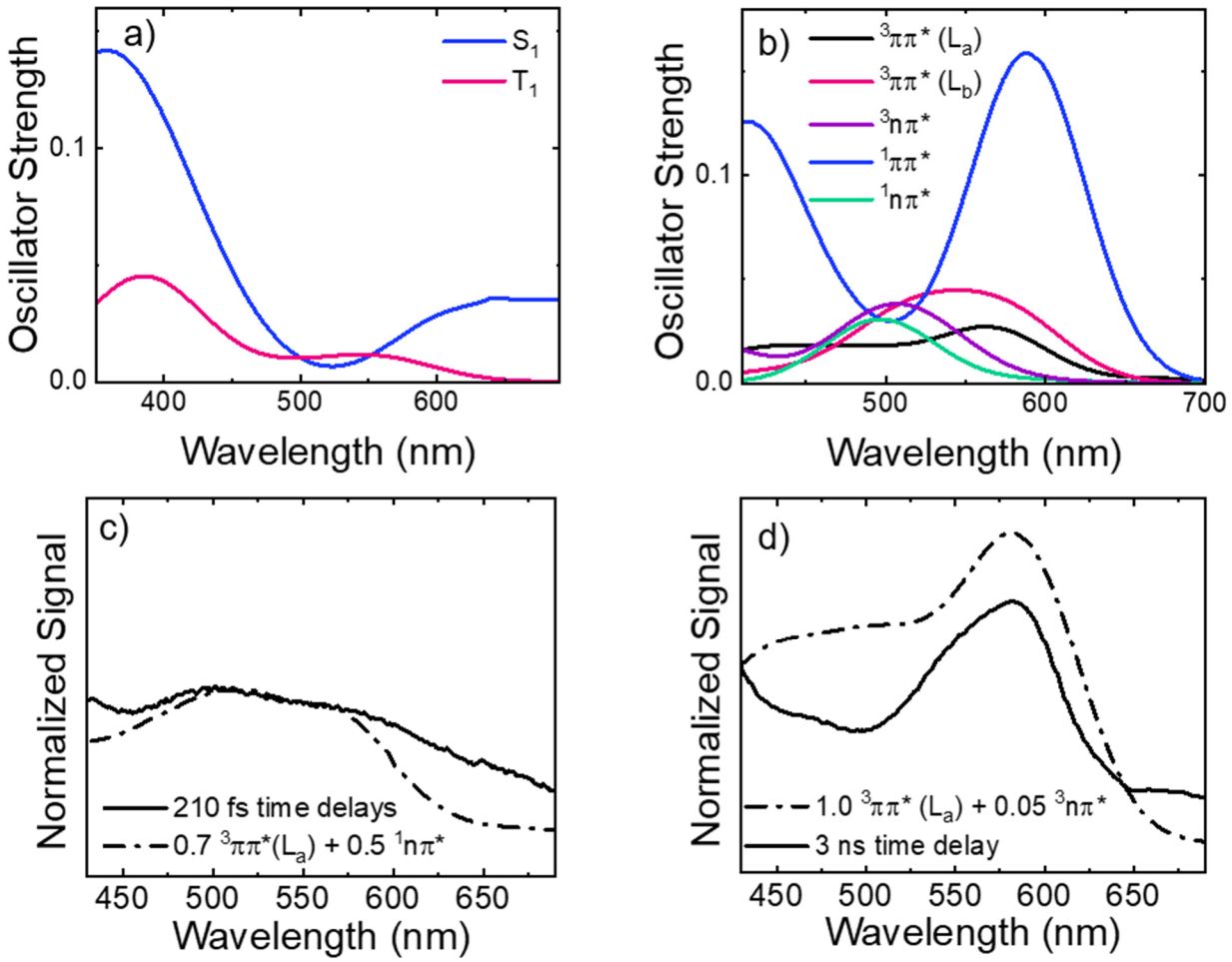

Figure S12. Calculated excited state absorption spectra for the a) $^1\pi\pi^*$ and $^3\pi\pi^*(T_1)$ minima of ThiaHX and b) the $^1\pi\pi^*$, $^1n\pi^*$, $^3\pi\pi^*$-L_a, $^3n\pi^*$ and $^3\pi\pi^*$-L_b minima of ThiathioHX at the CASPT2(12,10)/aug-cc-pVTZ/PCM level of theory in MeCN. Superposition of experimental transient absorption spectra (black, solid lines) and simulated ESA spectra (black dashed-dotted line) in MeCN (c and d). The calculated S_1 state ESA spectrum shown in panel a was shifted by -0.26 eV. The simulated d ESA spectra was shifted by -0.1 eV. The transitions used to generate the ESA spectra were convoluted with Gaussian functions with FWHM = 40 nm. A spectral range above 430 nm is shown in panels c and d because below 430 nm ThiathioHX absorbs and the bleaching signal cannot be modeled with the calculations.

S2.4 Femtosecond transient absorption

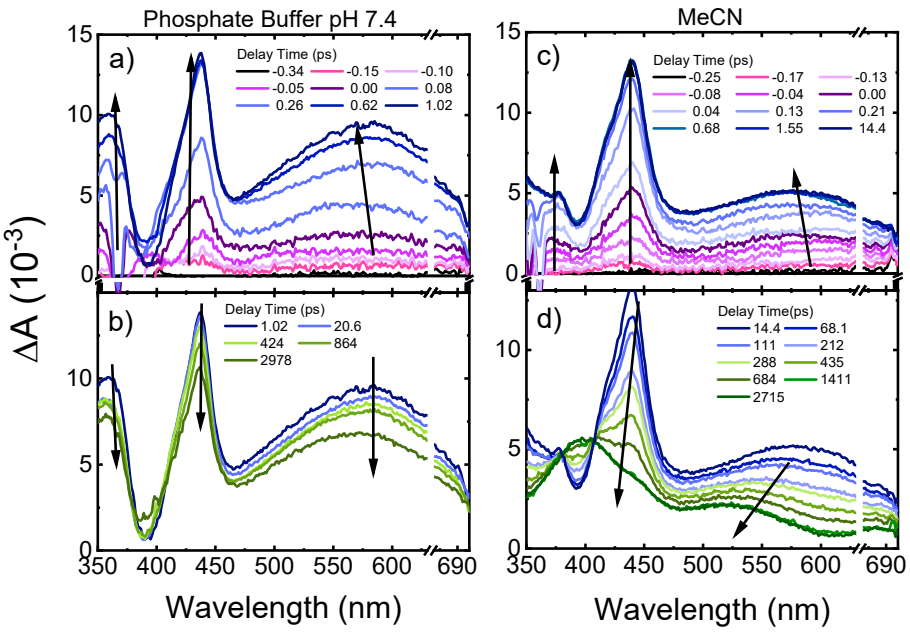

Figure S13. Transient absorption spectra of ThiaHX in phosphate buffer pH 7.4 (a & b) and in MeCN (c & d) upon excitation with 325 nm. Stimulated Raman emission from the solvent is observed at 367 nm within the cross-correlation of the pump-probe beams. The breaks are covering the overtone of the pump beam at 650 nm.

Figure S13 depicts the transient absorption spectra of ThiaHX in phosphate buffer pH 7.4 and in MeCN upon excitation at 325 nm (3.81 eV). Initially, a transient species with absorption maxima at 360, 437, and 582 nm is observed in phosphate buffer within the cross-correlation of the pump and probe laser beams, which continues to grow and slightly blueshifts to a time delay of 1 ps (Figure S13a). A depletion in excited state absorption is also observed around 390 nm, where the steady-state fluorescence of this thieno[3,4-*d*]pyrimidine derivative is observed (Figure S1). The transient species decays monotonically on a time scale longer than the 3 ns window reported in Figure S13b.

Figure S13 also depicts the fs-transient spectral evolution of ThiaHX in MeCN upon excitation at 325 nm. A transient absorption species is populated within 14 ps, which has

absorption band maxima at 376, 439, and 570 nm (Figure S13c). Additionally, the absorption band with maximum at 570 nm shows some blue shifting as it rises. Interestingly, a significant fraction of this transient species decays to populate another transient absorption species in hundreds of picoseconds, which has absorption maxima at ca. 400 and 530 nm (Figure S13d). Apparent isosbestic points are also observed at 377 and 407 nm, suggesting that indeed, the band with maxima at 400 and 530 nm corresponds to a new species. Table 1 collects the lifetimes extracted from the global and target analysis of ThiaHX in phosphate buffer and MeCN using a two-component sequential kinetic model, in which the second lifetime models the slow decay of the transient data in a time scale longer than 3 ns. Representative decay traces, best fits and EADS are shown in Figure 4.

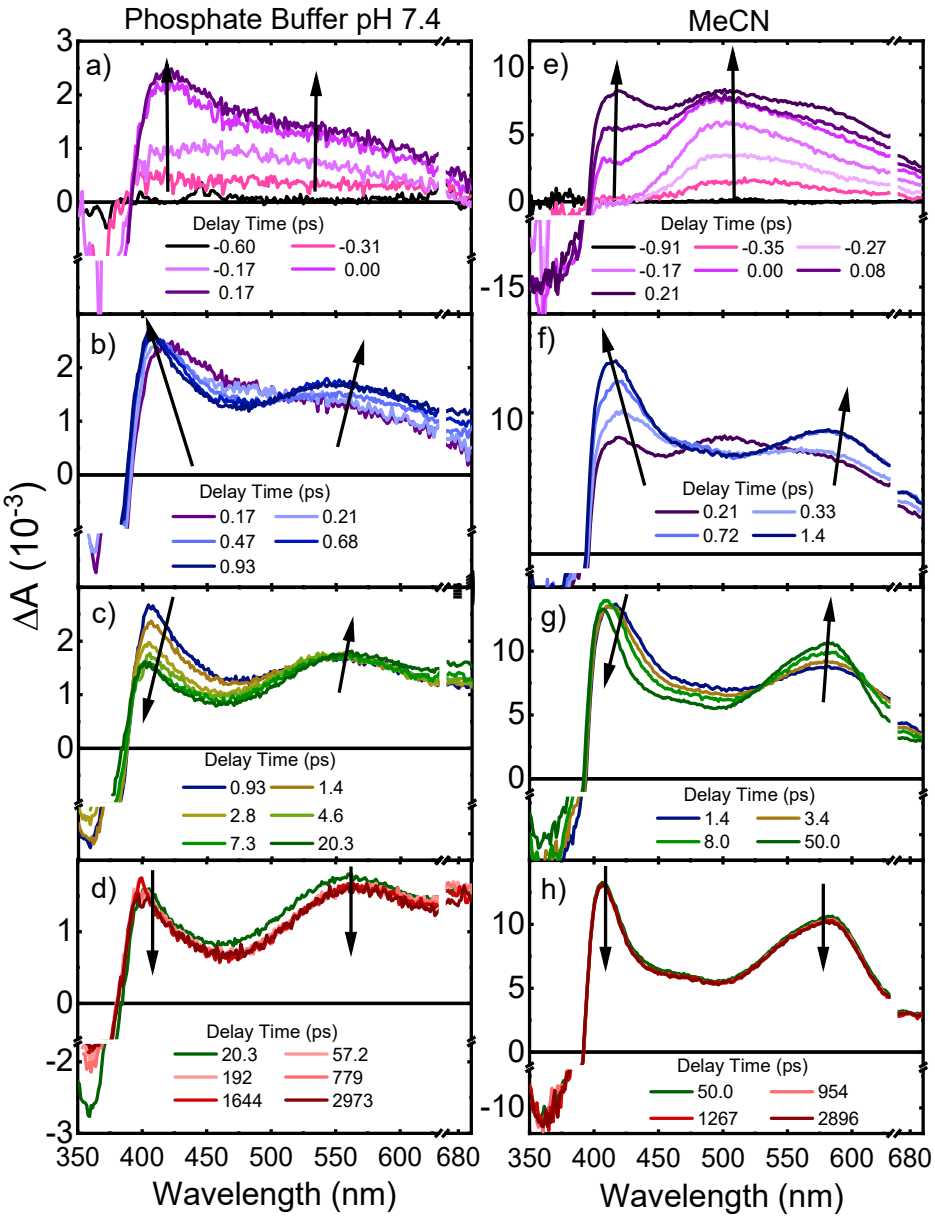

Figure S14. Transient absorption spectra of ThiathioHX in phosphate buffer pH 7.4 (a-d) and MeCN (e–h) upon excitation at 325 nm. Stimulated Raman emission from the solvent is observed at 367 nm within the cross-correlation of the pump-probe beams. The breaks are covering the overtone of the pump beam at 650 nm.

Figure S14a–d shows the transient absorption spectra of ThiathioHX in phosphate buffer pH 7.4 upon excitation at 325 nm. A broad transient absorption band in the range of 400 to 700 nm with no clear maximum grows within the cross-correlation of the pump and probe beams and

subsequently developing a maximum at ca. 400 nm and a shoulder at longer wavelengths than 450 nm (Figure S14a). Ground state depopulation is also observed at wavelengths shorter than 400 nm. The absorption band with maximum at ca. 400 nm slightly blueshifts and increases its amplitude, while another absorption band simultaneously grows with maxima at 550 nm (Figure S14b). An apparent isosbestic point is also observed at 510 nm, suggesting a state-to-state transition. From a delay time of 1 to 20 ps (Figure S14c), the transient absorption band maximum around 400 nm starts to decay with a simultaneous increase of the ground-state depopulation signal at wavelengths shorter than 400 nm, while the absorption band with maximum around 550 nm redshifts to ca. 565 nm. Additionally, a simultaneous increase in absorption at wavelengths larger than ca. 650 nm is observed for a delay time of up to 20 ps (Figure S14c), after which the transient species does not decay any further (Figure S14d) for up to 3 ns within experimental uncertainties. We remark that the apparent ground-state recovery observed during the first ca. 20 ps is possibly due to the population of transient species absorbing at wavelengths shorter than 450 nm and is not necessarily due to the repopulation of the ground state.

In addition, Figure S14e–h shows the transient absorption results for ThiathioHX in MeCN exciting at 325 nm. Within the cross-correlation of the pump and probe beams, a transient absorption signal with maximum at ca. 500 nm grows, subsequently also developing an absorption maximum at ca. 415 nm. The negative amplitude band observed below 400 nm is due to ground-state depopulation. The band with absorption maximum at 500 nm decays, while the band with absorption maxima around 420 and a band that forms with maximum at ca. 580 nm increases their amplitudes for up to ca. 1.4 ps (Figure S14f). Apparent isosbestic points are also observed at 476 and 541 nm. From 1.4 to 50 ps (Figure S14g), the band with absorption around 415 nm blueshifts, while the band at 580 nm increases and redshifts. From 50 ps to 3 ns, the transient species do not

decay significantly (Figure S14h). Table 1 collects the lifetimes extracted from the global and target analysis of ThiathioHX in phosphate buffer and MeCN using a two-component sequential kinetic model, in which the second lifetime models the slow decay of the transient data in a time delay much longer than 3 ns. Representative decay traces, best fits, and EADS are shown in Figure 5.

S2.5 Electronic relaxation mechanism of ThiaHX upon UVA photoactivation

A transient species is initially populated within the cross-correlation of the pump and probe beams in ThiaHX. This transient species has absorption maxima at 360, 439, and 582 nm in phosphate buffer and at 376, 439 and 570 nm in MeCN (Figure S13a). The CASPT2(12,10)/aug-cc-pVTZ calculations predict that the $^1\pi\pi^*$ state is populated upon excitation at 325 nm (Table S1). Additionally, the transient absorption signal resembles the calculated excited state absorption spectrum of the $^1\pi\pi^*$ state minimum (Figure S12a). Taking these observations together, we assign the transient absorption species to the excited state absorption spectrum of the $^1\pi\pi^*$ state.

In phosphate buffer, the transient band with absorption maximum at 582 nm grows and blueshifts for up to 1 ps (Figure S13a). This is likely due to a combination of intra- and intermolecular vibrational redistribution of the excess energy in the $^1\pi\pi^*$ state of ThiaHX. Thus, we assign the first lifetime to these processes. The observed transient absorption minimum around 390 nm is assigned to stimulated fluorescence emission from the $^1\pi\pi^*$ state population, in agreement with the fluorescence emission band observed in Figure S1a. The excited-state absorption spectrum of the $^1\pi\pi^*$ state decays on a time scale longer than the 3 ns time window reported in Figure S13b. This is further supported by the fluorescence quantum yield of ca. 30% measured in this solvent. The need to include a second decay lifetime to model the transient data

indicates that the fluorescence lifetime of ThiaHX is significantly longer than 3 ns. Interestingly, the transient absorption signal observed at ca. 376 nm increases its intensity as the transient signals at ca. 439 and 570 nm decay, which suggest that a different transient species is being populated as the $^1\pi\pi^*$ state decays. This can be clearly observed in the 383 nm decay traces shown in Figure 4 (i.e., the signal increases at late time delays). As shown in Figure S12a, the $^3\pi\pi^*(T_1)$ state absorbs strongly in the region of 350 to 500 nm. Therefore, we propose that a fraction of the population is crossing to the triplet manifold and populating the $^3\pi\pi^*(T_1)$ state.

To gain additional information regarding the triplet population, nanosecond transient absorption measurements and singlet oxygen quantum yield measurements were performed. The nanosecond transient absorption results (Figure S15 and Table 2), together with the singlet oxygen quantum yields measurements (Figure S16 and Table 2) confirm that ThiaHX populates the triplet manifold with a yield of at least 35% (considering the 35% singlet oxygen yield measured). We therefore propose that the electronic relaxation of ThiaHX in phosphate buffer occurs mainly through a combination of fluorescence (0.31 ± 0.02), and intersystem crossing that occurs within 3 ns, populating the reactive triplet state, which decays with a lifetime of 10 μs and sensitizes the generation of singlet oxygen with a yield of ca. 35%.

As in phosphate buffer, the growth and blue shift of the band at ca. 580 nm in MeCN are assigned to vibrational redistribution in the $^1\pi\pi^*$ state. Interestingly, in contrast with ThiaHX in phosphate buffer, the population of a long-lived transient species is detected very clearly in MeCN (Figure S13d), within the 3 ns temporal window of our femtosecond transient absorption measurements. The detection of a different transient species is supported by the observation of apparent isosbestic points at 377 and 407 nm. Theoretical

calculations predict the existence of a $^1\pi\pi^*/T_2(^3\pi\pi^*)$ crossing region that can be accessed in a barrierless fashion. The SOC at this crossing-region is small (i.e., 0.06 cm^{-1}) because both excited states have the same molecular orbital type, suggesting a relatively slow intersystem crossing pathway. The more evident intersystem crossing in MeCN, and lower fluorescence quantum yield, can be attributed to two factors. Firstly, a slightly higher SOC at the $^1\pi\pi^*/T_2(^3\pi\pi^*)$ crossing point (0.06 vs 0.03 cm^{-1}). And, secondly, the fact that the potential energy surfaces of the $^1\pi\pi^*$ and $T_2(^3\pi\pi^*)$ states remain nearly isoenergetic throughout, as illustrated in the FC→$^1\pi\pi^*$ minimum LIIC paths (Figures S8 and S9). The ensuing transient absorption signal resembles the calculated excited state absorption spectrum of the $T_1(^3\pi\pi^*)$ state minimum (Figure S12).

Nanosecond transient absorption and singlet oxygen measurements confirm that triplet population occurs with a yield of at least 50%, considering the measured singlet oxygen quantum yields. We therefore propose that at least 50% of the $^1\pi\pi^*$ state population intersystem crosses to populate the triplet manifold in hundreds of picoseconds. The population reaching the $T_2(^3\pi\pi^*)$ state then decays to the lower $T_1(^3\pi\pi^*)$ state via a T_2/T_1 conical intersection region, because such process only needs to overcome a barrier of 0.05 eV (Figure 3a). Consequently, the $T_2(^3\pi\pi^*)$ state internally converts in ultrafast time scale through a T_2/T_1 conical intersection to populate the $T_1(^3\pi\pi^*)$ state, which decays with a lifetime of 15 μs and sensitizes the generation of singlet oxygen. Finally, no significant degradation (7%) was observed following an irradiation dose of 190 J cm^{-2}. The proposed deactivation mechanisms are reported in Scheme S1.

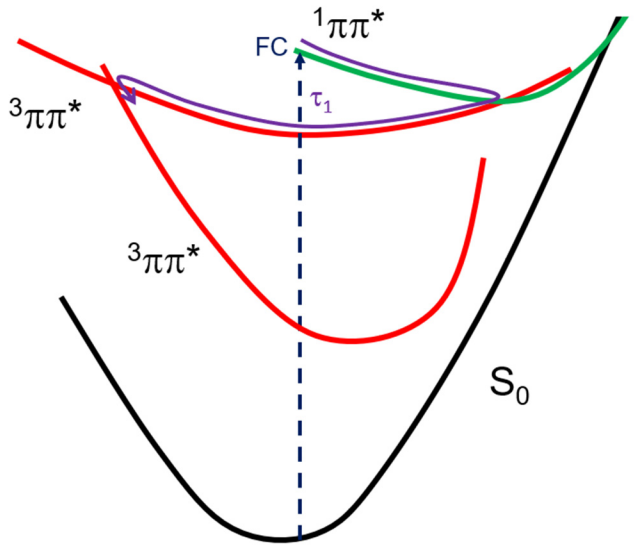

Scheme S1. Proposed excited-state relaxation mechanisms for ThiaHX based on the calculations and experiments reported in this work**.**

S2.6 Nanosecond transient absorption

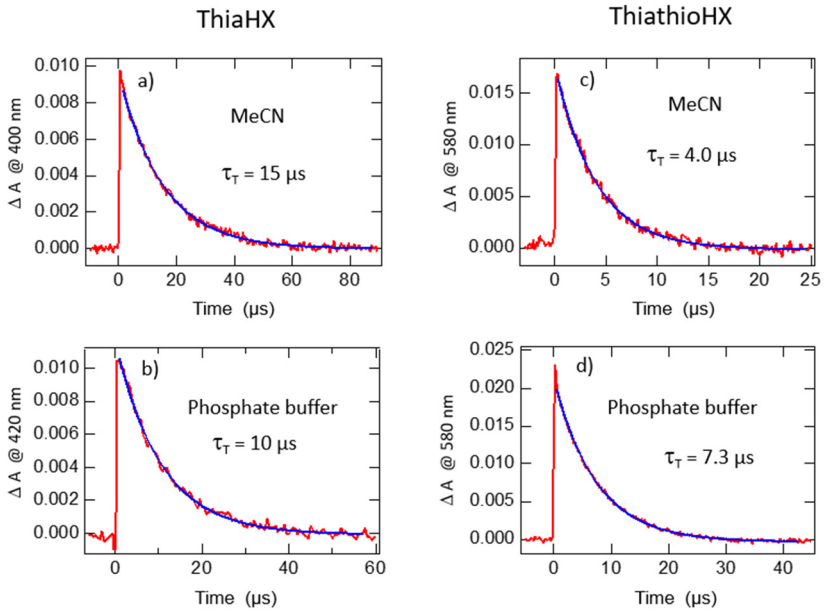

Figure S15. Triplet absorption decay traces of argon-purged solutions of ThiaHX (a, b) and ThiathioHX (c, d) in MeCN (a, c) and phosphate buffer at pH 7.4 (b, d) after pulsed laser excitation at 308 nm (a, b) or 355 nm (c, d).

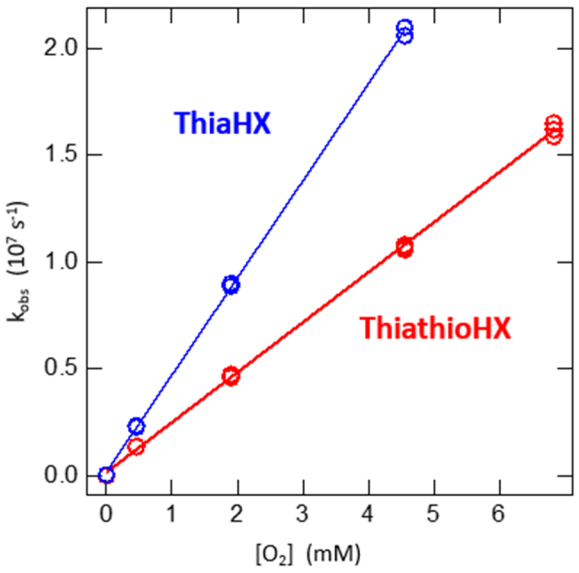

Figure S16. Determination of the bimolecular quenching rate constants k_q^{O2} of quenching of ThiaHX and ThiathioHX triplet states by molecular oxygen using laser flash photolysis (λ_{ex} = 308 nm for ThiaHX and 355 nm for ThiathioHX). Pseudo-first-order decay rate constant of ThiaHX and ThiathioHX triplet state absorbance monitored at 525 nm (ThiaHX) and at 580 nm (ThiathioHX) vs. varying concentration of dissolved molecular oxygen in acetonitrile.

S2.7 Singlet oxygen generation yields

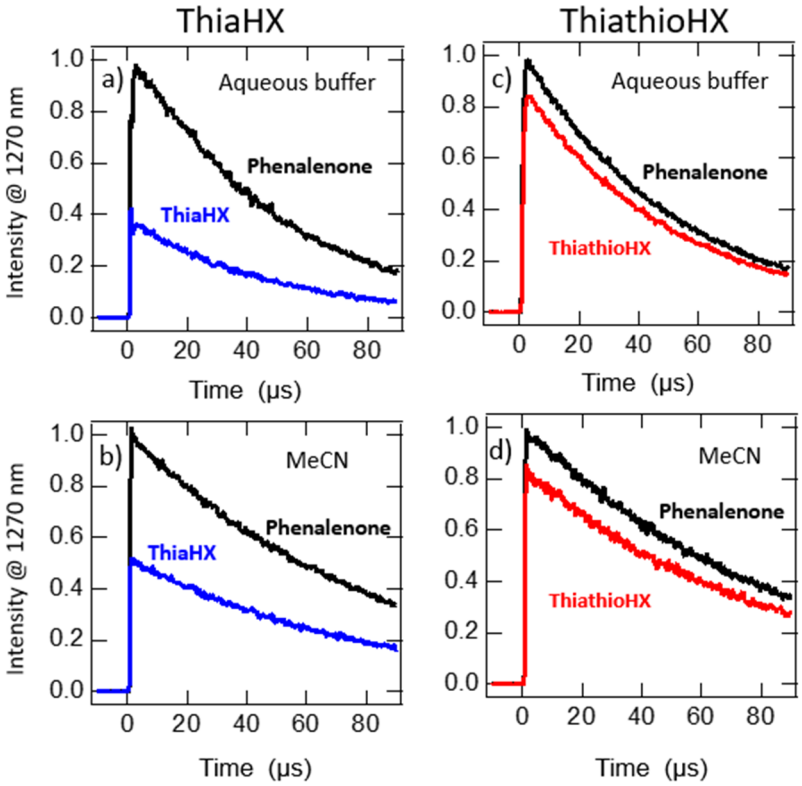

Figure S17. Singlet oxygen phosphorescence decay traces monitored at 1270 nm generated by pulsed photoexcitation (308 nm for ThiaHX and 355 nm for ThiathioHX) of ThiaHX (69.3 µM or 71.6 µM) and ThiathioHX (29.8 µM or 34.2 µM), respectively in O_2-saturated D_2O buffer solution (Tris 10 mM, pH=7.5) (a, c) and in O_2-saturated MeCN (b, d).

S2.8 Intracellular fluorescent intensities of ROS sensor DCF-DA

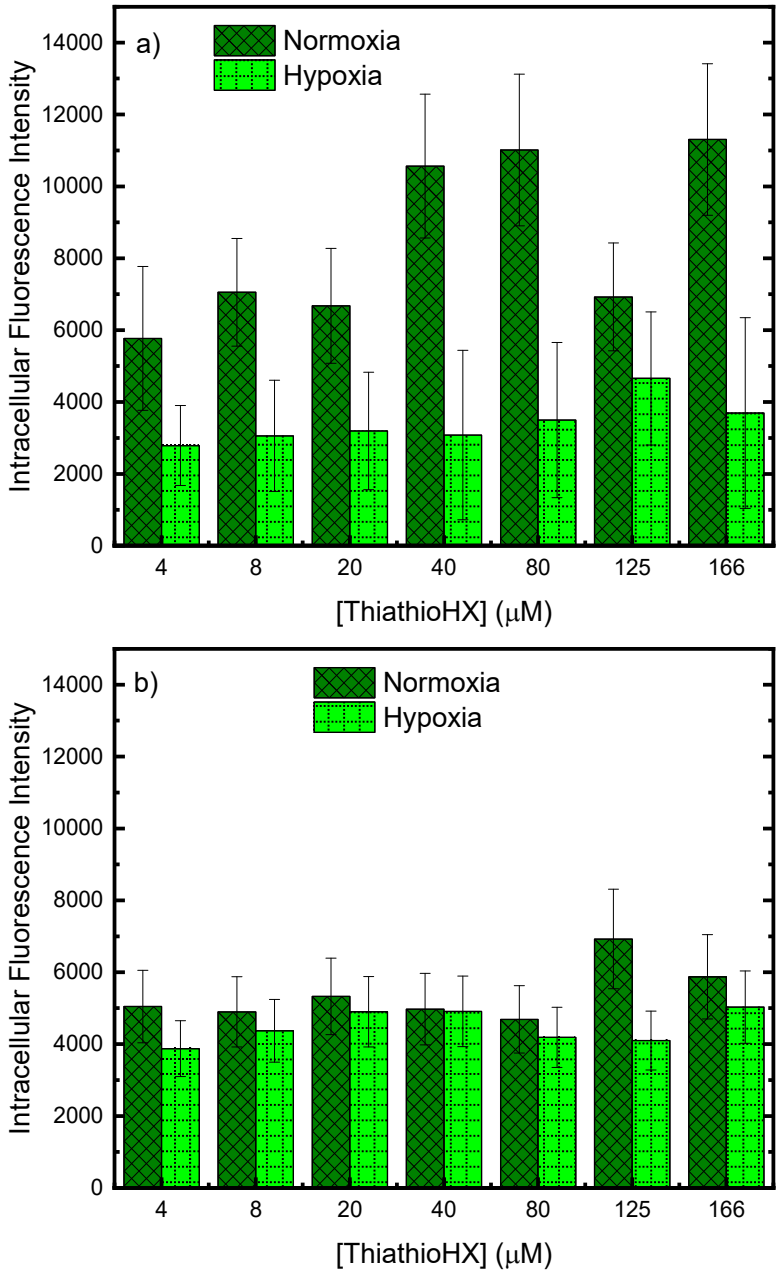

Figure S18. Intracellular fluorescent intensities of ROS sensor DCF-DA in a) B16F10 and b) HeLa cells without UVA irradiation.

S2.9 Photoirradiation of ThiathioHX in the presence and absence of calf thymus DNA

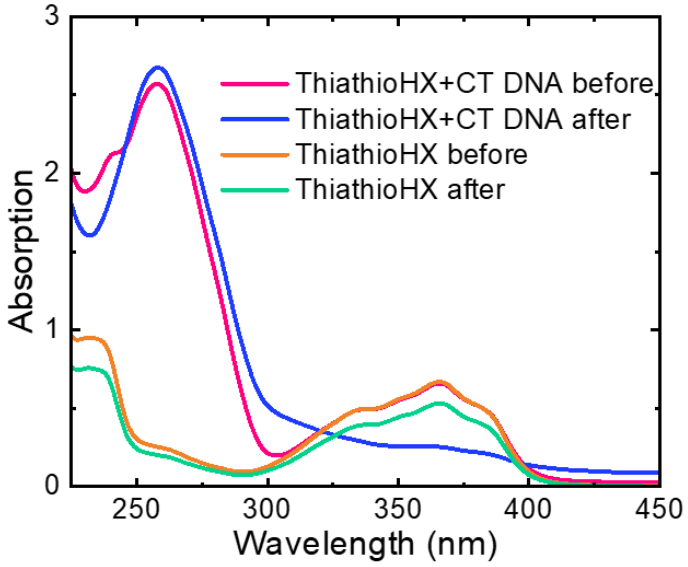

Figure S19. Absorption spectra of N_2(g)-purged ThiathioHX in absence and presence of calf thymus (CT) DNA before and after laser irradiation with a dose of 300 J cm^{-2} (λ_{exc} = 325 nm) in phosphate buffer pH 7.4. Concentrations of ThiathioHX and CT DNA were 0.06 mM and 0.4 mM, respectively. Solutions were deoxygenated before irradiation with N_2(g) for 30 minutes. Note that the irradiation of N_2(g)-purged mixture of ThiathioHX and CT DNA solution leads to significant changes in the absorption spectra of both CT DNA and ThiothioHX, hence, supporting the idea of photocrosslinking or photocycloaddition reactions between ThiothioHX and CT DNA in the absence of O_2.

S2.10 Lamp emission spectrum and transmittance spectrum of the plates

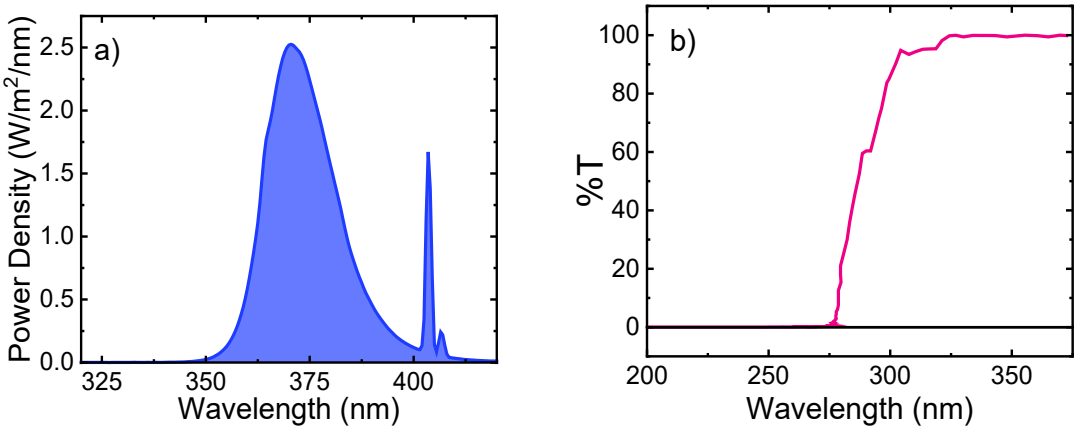

Figure S20. a) Emission spectrum of the UVA lamp used in the *in vitro* studies and b) Transmittance spectrum of the polystyrene plates used in this work.

S2.11 Additional computational figures and active spaces

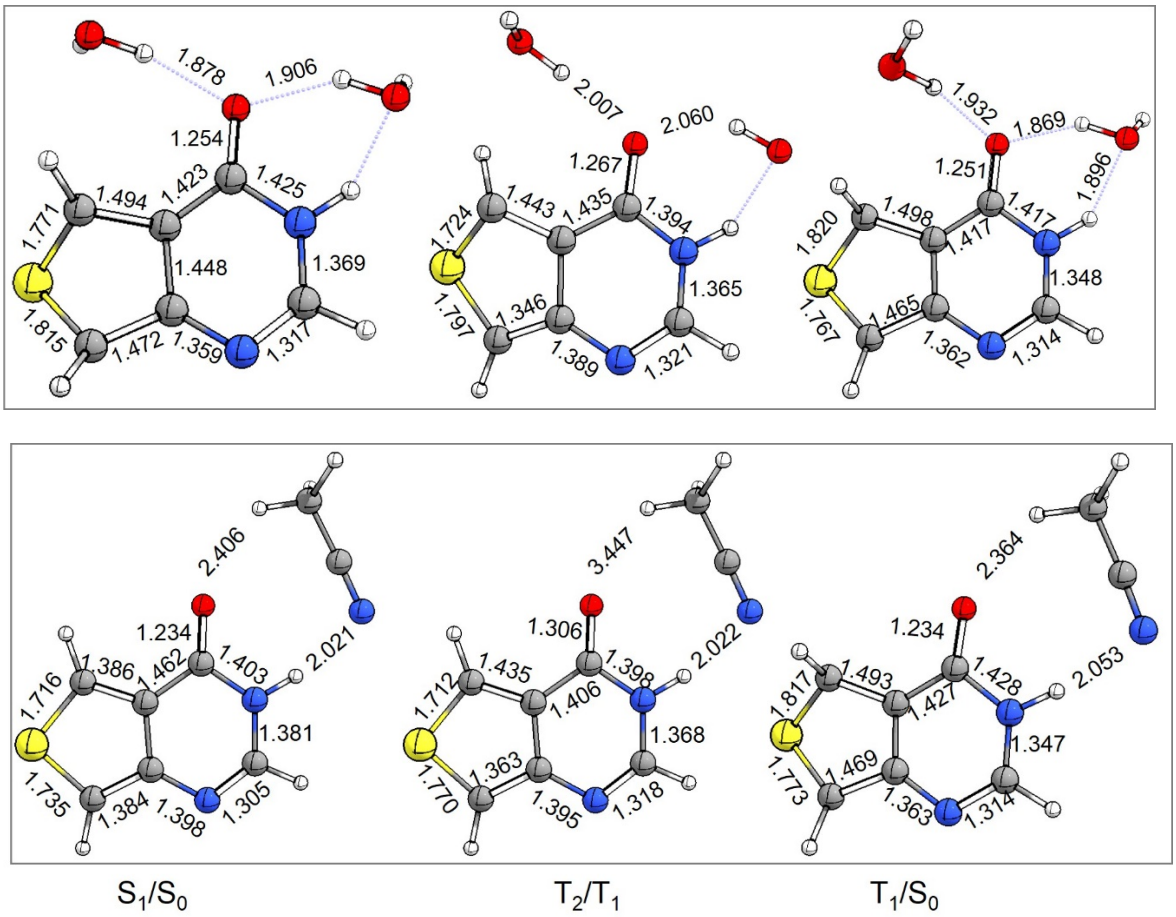

Figure S21. Conical intersection structure of ThiaHX optimized at the CASPT2/cc-PVDZ level in the presence of water (top) and MeCN (bottom). Selected bond lengths are presented in angstroms.

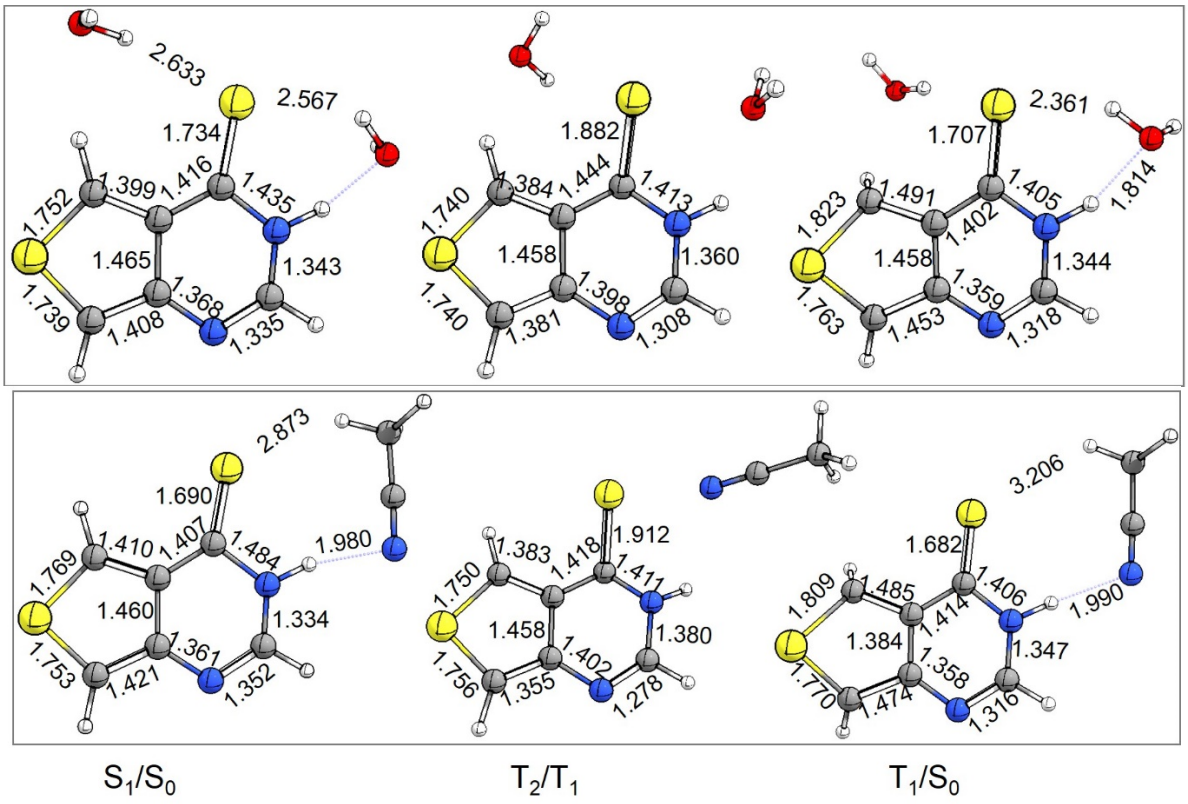

Figure S22. Intersection structures of ThiathioHX optimized at the CASPT2/cc-PVDZ level in the presence of water (top) and MeCN (bottom). Selected bond lengths are presented in angstroms.

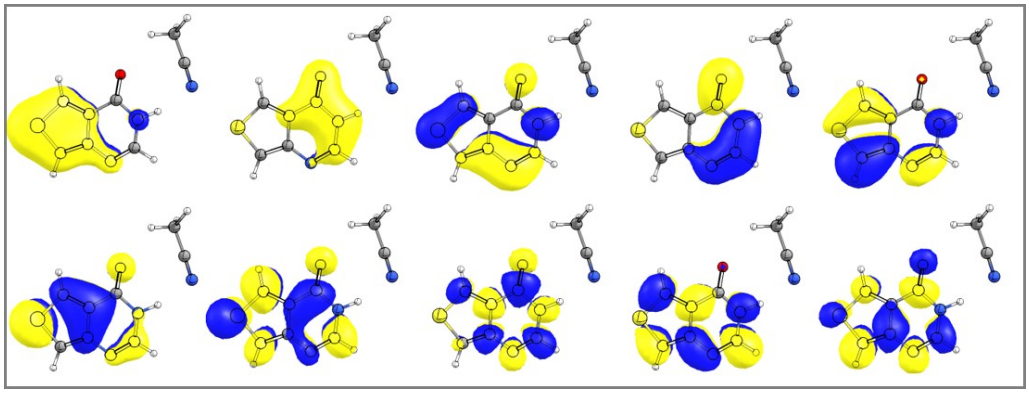

Figure S23. The active space of 12 electrons in 10 orbitals used in the CASPT2/cc-PVDZ level of theory calculations of ThiaHX in MeCN.

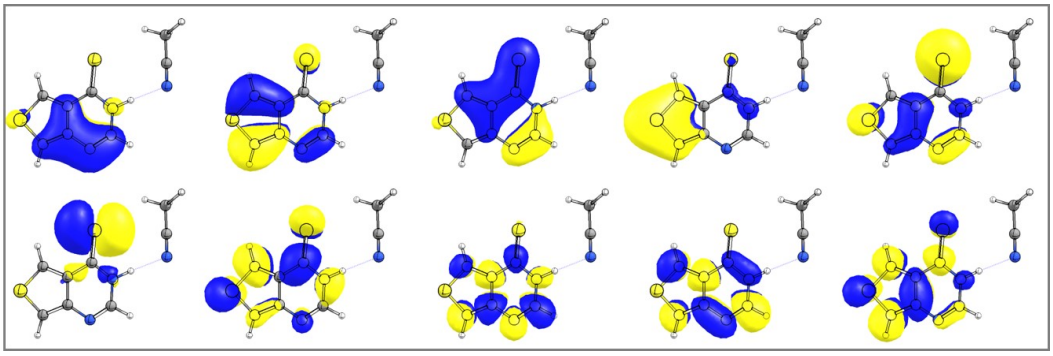

Figure S24. The active space of 12 electrons in 10 orbitals used in the CASPT2/cc-PVDZ level of theory calculations of ThiathioHX in MeCN.

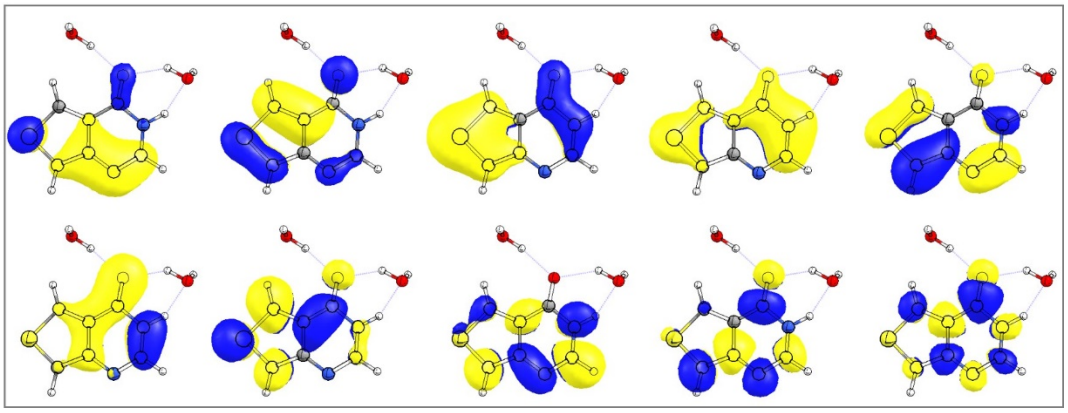

Figure S25. The active space of 12 electrons in 10 orbitals used in the CASPT2/cc-PVDZ level of theory calculations of ThiaHX in water.

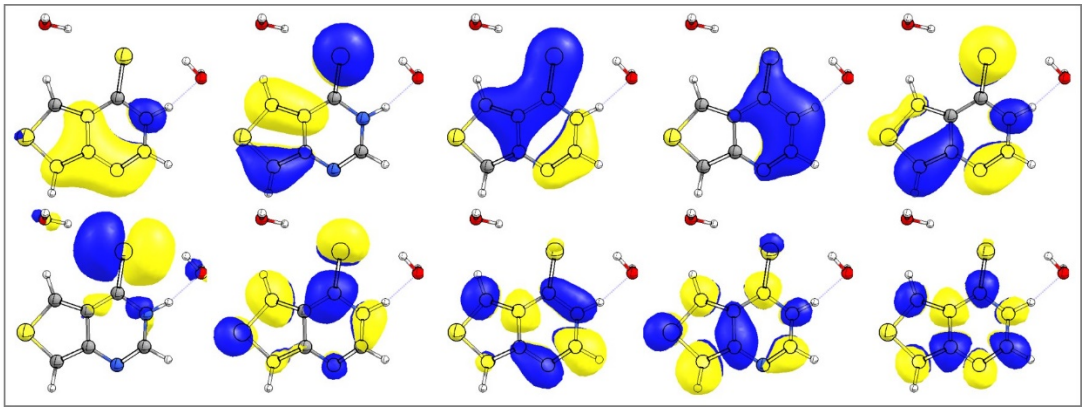

Figure S26. The active space of 12 electrons in 10 orbitals used in the CASPT2/cc-PVDZ level of theory calculations of ThiathioHX in water.

S3 Synthesis and characterization of Thieno[3,4-d]pyrimidin-4(1H)-one (ThiaHX) and Thieno[3,4-d]pyrimidin-4(1H)-thione (ThiathioHX)

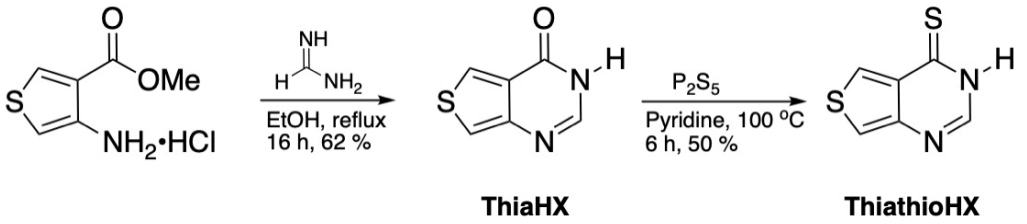

S3.1 Procedures

Thieno[3,4-d]pyrimidin-4(1H)-one (ThiaHX)

To a flame dried round bottom flask purged with argon was added methyl 4-aminotiophene-3-carboxylate hydrochloride (1.0 g; 5.2 mmol), EtOH (10 ml) and formamide acetate (1.6 g; 15.4 mmol; 3 eq). The solution was refluxed at 95°C overnight. Upon cooling, the precipitate was filtered and washed with EtOH and cold H_2O. The solid is dried under *vacuum* in presence of P_2O_5 to yield a light brown powder (0.49 g; 3.2 mmol, 62% yield). A sample was recrystallized, and a high-resolution X-ray crystal structure was obtained (see below).

Rf = 0.4 (5% MeOH:CH_2Cl_2)
^{1}H-NMR (300 MHz, DMSO-*d*$_6$) δ 11.65 (s, 1H), 8.47 (d, *J* = 3.2 Hz, 1H), 7.80 (d, *J* = 3.3 Hz, 1H), 7.78 (d, *J* = 3.5 Hz, 1H).
^{13}C-NMR (100 MHz, DMSO-*d*$_6$) δ 157.87, 148.57, 143.74, 127.92, 126.44, 118.33.
ESI-HRMS : calculated for $[C_6H_3N_2OS]^+$ $[M-H]^+$ 153.0117 , found 153.0114 ; delta (ppm)=-2.0

Thieno[3,4-d]pyrimidin-4(1H)-thione (ThiathioHX)

In a flame dried round bottom flask purged with argon, ThiaHX (0.2 g; 1.3 mmol) is dissolved in pyridine (10 ml). P_2S_5 (1 g, 5 × 0.2 g) is added in portions every hour and the solution is heated at 100°C for a total of 6 h (until all starting material is consumed). The volatiles are evaporated under high vacuum and water (10 ml) is added to give and an orange suspension, which is basified with 40% NaOH to pH 12–13 **(**suspension should dissipate). The solution is then neutralized with 37% HCl, and a yellowish precipitate forms, which is subsequently isolated by filtration. The solid is then washed with cold H_2O and dried over P_2O_5 under *vacuum* to yield a yellow fluffy solid (0.12 g, 0.69 mmol, 50 % yield). A sample was recrystallized, and a high-resolution X-ray crystal structure was obtained (see below).

Rf = 0,4 (5%MeOH in CH_2Cl_2)
^{1}H-NMR (300 MHz, DMSO-*d*$_6$) δ 13.23 (s, 1H), 8.59 (d, *J*=3.3Hz, 1H), 7.95 (d, *J*=3.3Hz, 1H), 7.85 (s, 1H) ppm
^{13}C-NMR (100 MHz, DMSO-*d*$_6$) δ 182.53, 143.45, 141.51, 132.92, 130.32, 119.71 ppm
ESI-HRMS calculated for $[C_6H_3N_2S_2]^-$ $[M–H]^-$ 166.9743 , found 166.9744 ; delta (ppm)=0.6.

S3.2 NMR data

Compound 1 - thieno[3,4-d]pyrimidin-4(1H)-one : ThiaHX

^{1}H NMR

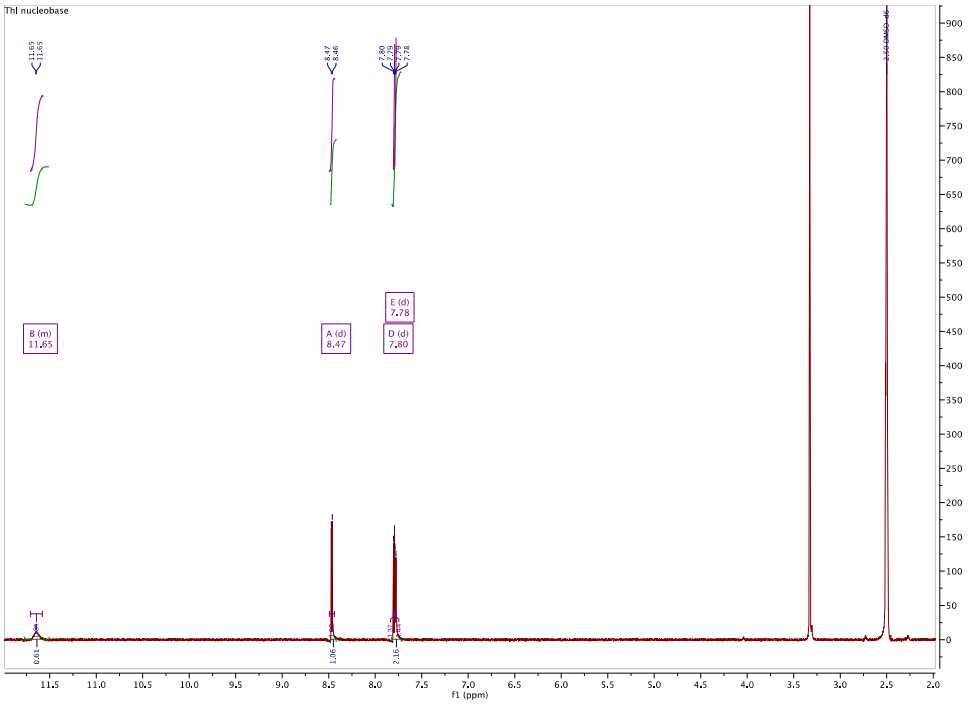

^{13}C NMR

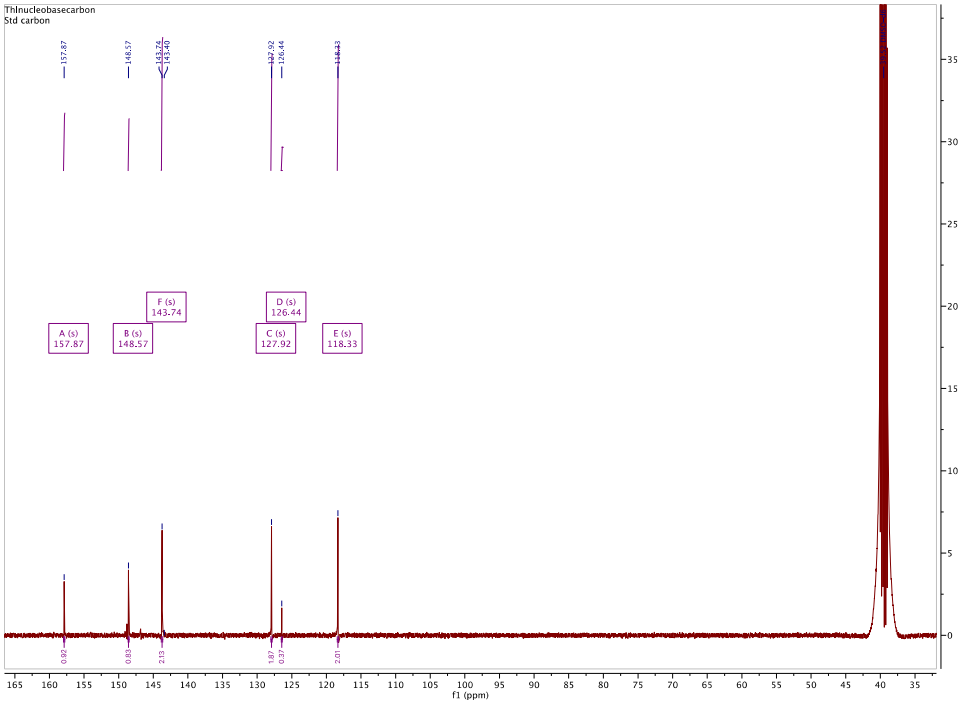

Compound 2 - thieno[3,4-d]pyrimidin-4(1H)-thione : ThiathioHX

^{1}H NMR

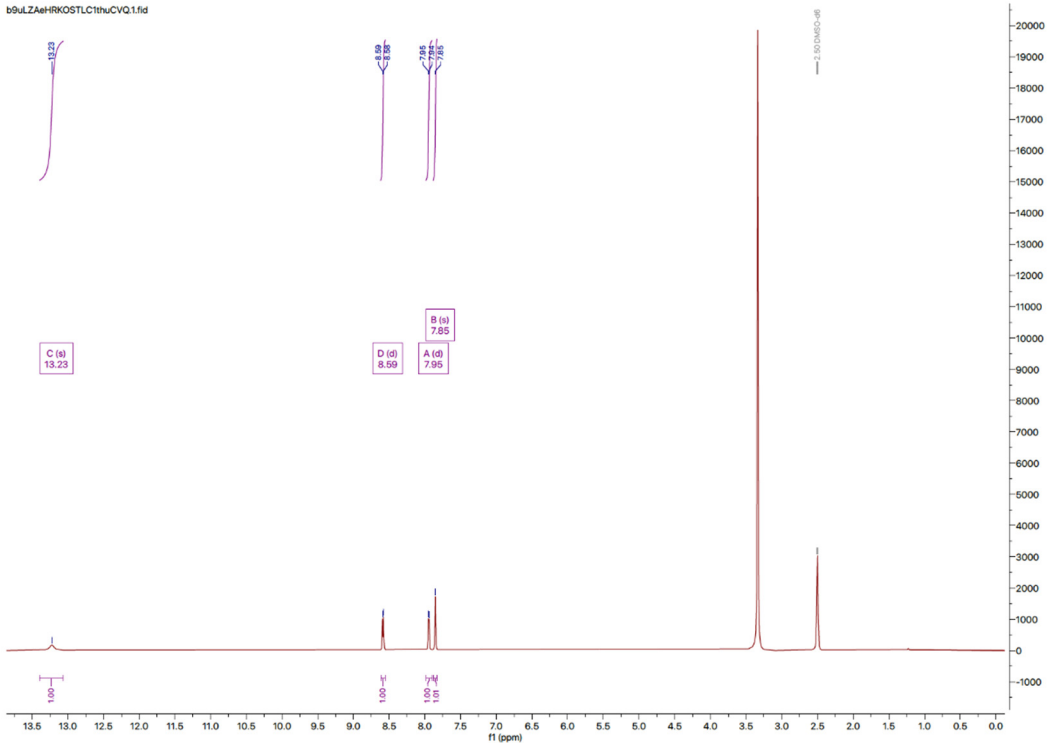

^{13}C NMR

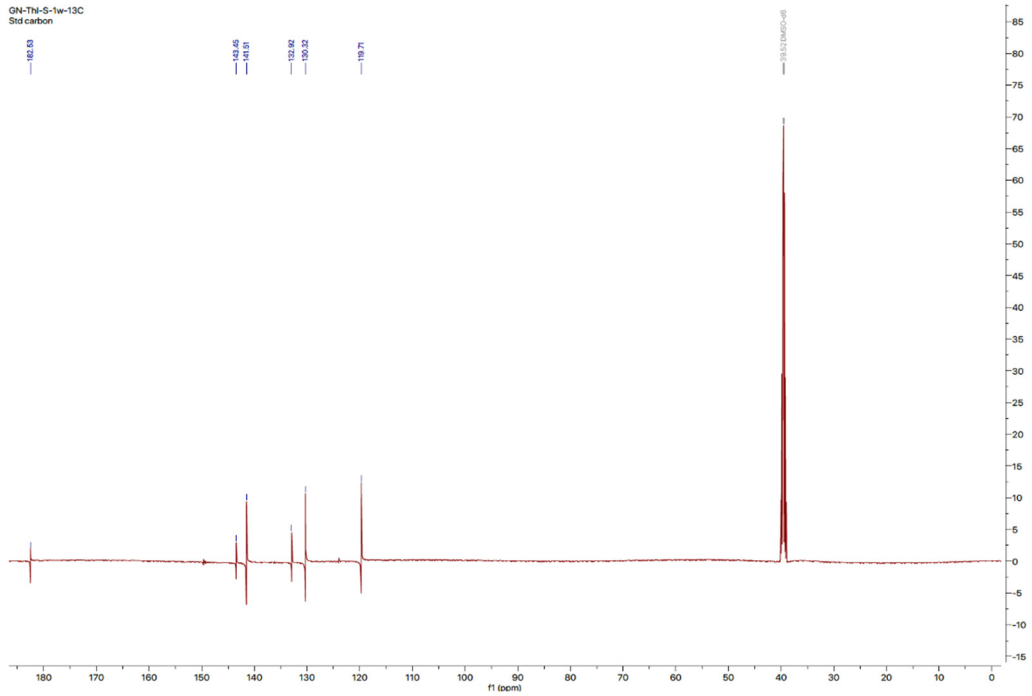

S3.3 High-resolution mass spectroscopy

Compound 1 - thieno[3,4-d]pyrimidin-4(1H)-one : ThiaHX

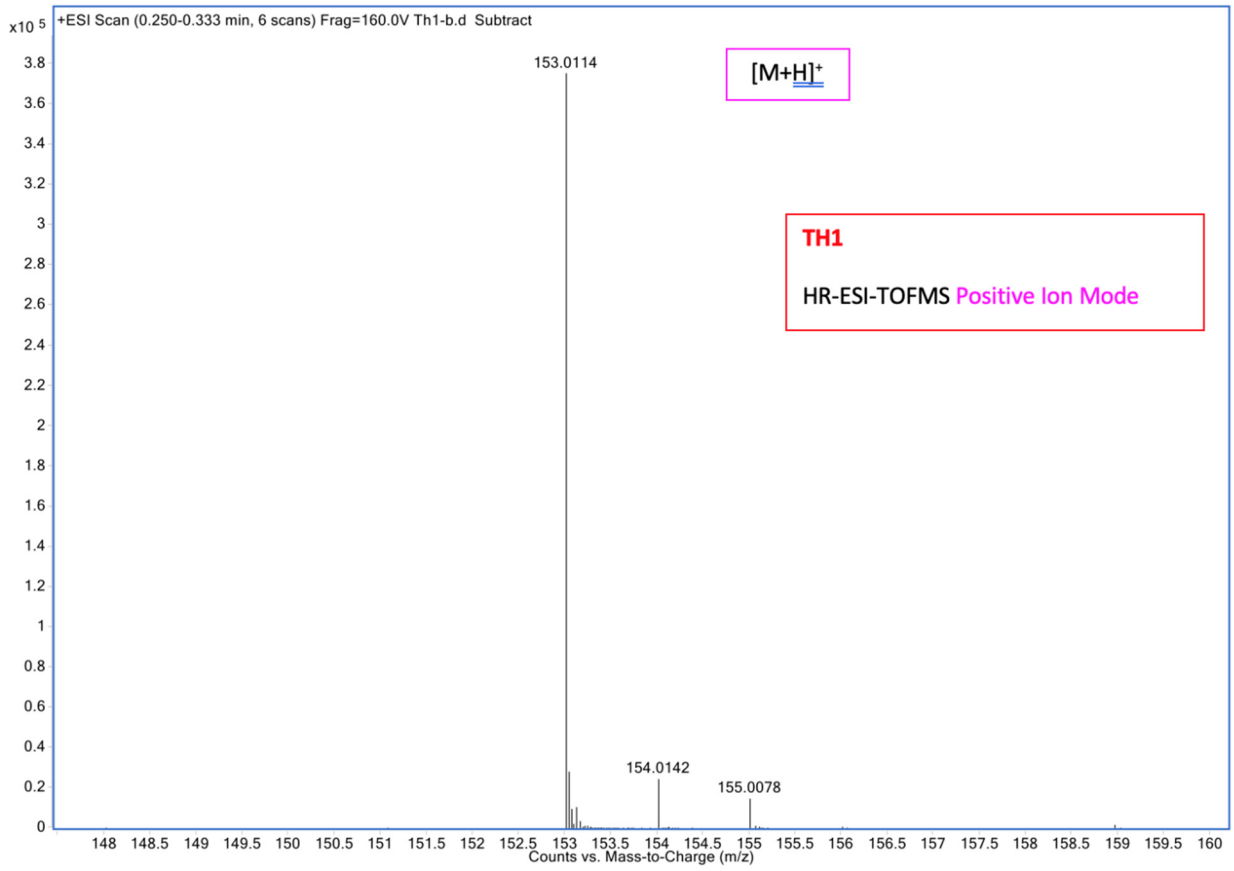

Search Results: Sample TH1

Mass Measured	Theo. Mass	Delta (ppm)	Composition
153.0114	153.0117	-2.0	$[C_6 H_5 N_2 O S]^+$

Compound 2 - thieno[3,4-d]pyrimidin-4(1H)-thione : ThiathioHX

HR-MS :

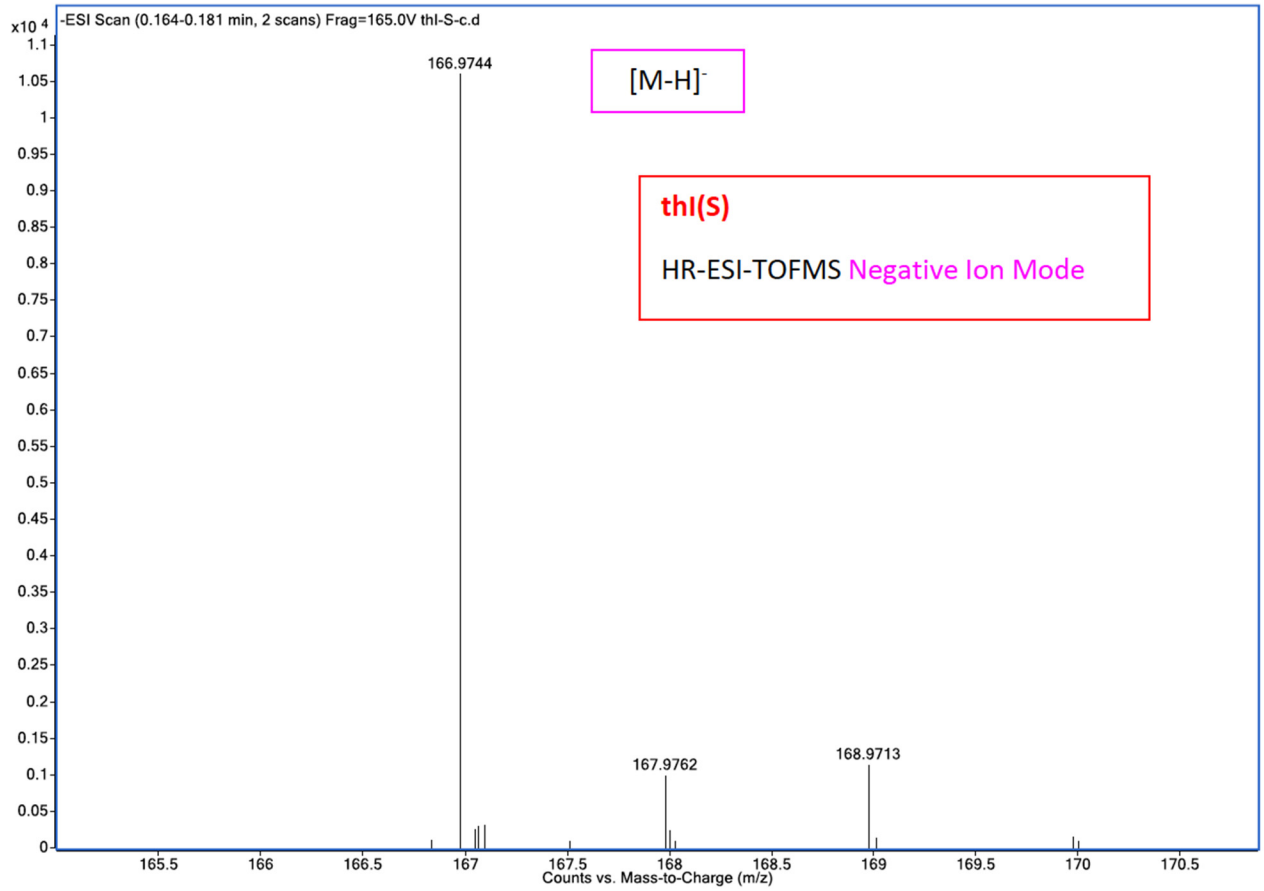

Search Results: Sample thI(S)

Mass Measured	Theo. Mass	Delta (ppm)	Composition
166.9744	166.9743	0.6	$[C_6 H_3 N_2 S_2]^-$

S3.4 X-ray structures

Compound 1 - thieno[3,4-d]pyrimidin-4(1H)-one : ThiaHX

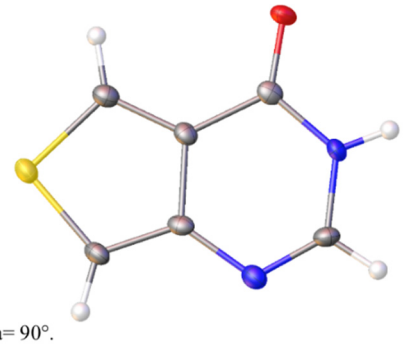

a= 90°.

b= 102.809(5)°.

g = 90°.

Report date	2019-05-30
Identification code	tor_thinb
Empirical formula	C6 H4 N2 O S
Molecular formula	C6 H4 N2 O S
Formula weight	152.17
Temperature	100.0 K
Wavelength	0.71073 Å
Crystal system	Monoclinic
Space group	P 1 21/n 1
Unit cell dimensions	a = 13.0765(12) Å
	b = 3.7722(4) Å
	c = 25.105(2) Å
Volume	1207.5(2) $Å^3$
Z	8
Density (calculated)	1.674 Mg/m^3
Absorption coefficient	0.447 mm^{-1}
F(000)	624
Crystal size	0.3 x 0.1 x 0.05 mm^3
Crystal color, habit	clear colourless needle
Theta range for data collection	1.629 to 26.361°.
Index ranges	-16<=h<=16, -4<=k<=4, -31<=l<=31
Reflections collected	7242
Independent reflections	2454 [R(int) = 0.0471]
Completeness to theta = 25.242°	99.5 %
Absorption correction	Semi-empirical from equivalents
Max. and min. transmission	0.4908 and 0.4178
Refinement method	Full-matrix least-squares on F^2
Data / restraints / parameters	2454 / 2 / 190
Goodness-of-fit on F^2	1.049
Final R indices [I>2sigma(I)]	R1 = 0.0462, wR2 = 0.0870
R indices (all data)	R1 = 0.0734, wR2 = 0.0948
Extinction coefficient	n/a
Largest diff. peak and hole	0.345 and -0.278 e.$Å^{-3}$

Compound 2 - thieno[3,4-d]pyrimidin-4(1H)-thione : ThiathioHX

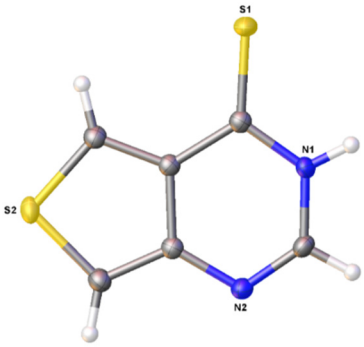

α= 90°.
β= 100.375(15)°.
γ = 90°.

Identification code	TOR_thI(S).nb
Empirical formula	C6 H4 N2 S2
Formula weight	168.23
Temperature	100.0 K
Wavelength	0.71073 Å
Crystal system	Monoclinic
Space group	P 21/c
Unit cell dimensions	a = 10.523(5) Å
	b = 9.208(4) Å
	c = 7.108(3) Å
Volume	677.4(5) $Å^3$
Z	4
Density (calculated)	1.650 Mg/m^3
Absorption coefficient	0.694 mm^{-1}
F(000)	344
Crystal size	0.22 x 0.08 x 0.05 mm^3
Theta range for data collection	1.967 to 26.349°.
Index ranges	-13<=h<=12, -11<=k<=11, -7<=l<=8
Reflections collected	6714
Independent reflections	1385 [R(int) = 0.0271]
Completeness to theta = 25.242°	100.0 %
Absorption correction	Semi-empirical from equivalents
Max. and min. transmission	0.7454 and 0.6453
Refinement method	Full-matrix least-squares on F^2
Data / restraints / parameters	1385 / 0 / 91
Goodness-of-fit on F^2	1.065
Final R indices [I>2sigma(I)]	R1 = 0.0258, wR2 = 0.0681
R indices (all data)	R1 = 0.0296, wR2 = 0.0704
Extinction coefficient	n/a
Largest diff. peak and hole	0.380 and -0.170 $e.Å^{-3}$

S4 Cartesian coordinates

20
ThiaHX_WAT_S0-MIN

O	-1.75771234	2.06840696	0.03581977
C	-1.36381460	0.88462790	0.00646316
N	-2.25630871	-0.16599555	-0.06628676
C	-1.89914417	-1.50044975	-0.15668637
N	-0.68568715	-1.97568880	-0.14632291
C	0.30197931	-0.99977673	-0.03753427
C	1.66205191	-1.25432190	-0.00163194
S	2.57059968	0.20914405	0.13181616
C	1.16596068	1.20574353	0.13566592
C	0.02564033	0.42733458	0.04117414
H	-3.25032509	0.11377694	-0.09056999
H	-2.74468671	-2.19009763	-0.24881392
H	1.22548035	2.29490136	0.20725592
H	2.15470183	-2.22591272	-0.03935235
O	0.15633162	4.21453775	0.15663578
H	0.18778075	4.39199483	-0.79286891
H	-0.58100833	3.57848531	0.20584982
O	-4.51039962	1.49011521	-0.08755449
H	-3.70445211	2.04328049	-0.10738643
H	-4.88433672	1.70343688	0.77839302

20
ThiaHX_WAT_S1-MIN

O	-1.81876164	2.10994331	-0.10537409
C	-1.35764935	0.94073927	0.24337199
N	-2.29849004	-0.19795217	0.02058474
C	-1.92904392	-1.44959675	-0.12495120
N	-0.65800635	-1.94626533	-0.08212904
C	0.29082297	-0.96841795	0.01562291
C	1.66998375	-1.23052050	-0.00057145
S	2.66308359	0.20160356	0.07356228
C	1.17725469	1.18083267	0.12353504
C	0.02542797	0.46103780	0.08513637
H	-3.29295487	0.09802100	-0.01403349
H	-2.72913342	-2.18074829	-0.29913537
H	1.24387736	2.27574414	0.18507887
H	2.11159368	-2.22509619	-0.10805182
O	0.10911064	4.10498956	0.08515987

H	0.12698349	4.38845085	-0.83845700
H	-0.65839229	3.49169148	0.08067872
O	-4.46568068	1.48417172	-0.05882718
H	-3.62067054	1.98338367	-0.16150768
H	-4.77670418	1.79153092	0.80437287
20			
ThiaHX_WAT_T1-MIN			
O	-1.76645519	2.06398714	0.01353092
C	-1.32860808	0.90468663	0.03353451
N	-2.27421744	-0.19238375	0.00526820
C	-1.92882266	-1.47083526	-0.11687514
N	-0.65055775	-1.94232645	-0.13832635
C	0.28068356	-0.98019250	-0.03171514
C	1.68439553	-1.26283357	-0.02228753
S	2.68975456	0.15047181	0.12292844
C	1.20608170	1.20451560	0.14007450
C	0.02189884	0.44042205	0.07584730
H	-3.26579266	0.11764820	-0.01680109
H	-2.74164042	-2.19946768	-0.20094477
H	1.29083933	2.29034160	0.22212585
H	2.10797979	-2.26560313	-0.09483793
O	0.11672650	4.25626794	0.17238206
H	0.19334028	4.37133772	-0.78378724
H	-0.60621041	3.60518765	0.22577414
O	-4.49355853	1.45211576	-0.16208159
H	-3.72071057	2.05021481	-0.13418768
H	-5.00247541	1.71998810	0.61444392
20			
ThiaHX_WAT_T2-MIN			
O	-1.74385989	2.05210288	0.06219919
C	-1.36574261	0.85526192	0.00785649
N	-2.28318571	-0.18404155	-0.09365522
C	-1.93544690	-1.49585810	-0.16890529
N	-0.67453574	-1.97527021	-0.15227689
C	0.29921079	-1.01755459	-0.03920075
C	1.66961491	-1.25407010	-0.00048991
S	2.60482665	0.24002936	0.15466759
C	1.19019887	1.22558457	0.14510364
C	0.00745843	0.41622134	0.04176855
H	-3.27360874	0.11581226	-0.10966863
H	-2.76243468	-2.20529500	-0.25196533

H	1.22864479	2.31225705	0.24163054
H	2.16913921	-2.22144722	-0.05277347
O	0.14728239	4.25745579	0.13212096
H	0.22358098	4.34273338	-0.82750038
H	-0.57116869	3.60442479	0.20762239
O	-4.50046163	1.49212761	-0.07696199
H	-3.70113209	2.05530082	-0.06715030
H	-4.91572943	1.69776767	0.77164414

20
ThiaHX_WAT_S1/S0

O	-1.86528231	2.10144782	-0.04498576
C	-1.40522534	0.94732731	0.12816449
N	-2.31157293	-0.14812574	0.21912983
C	-1.92693930	-1.46189071	0.21231174
N	-0.68965780	-1.91198617	0.22228128
C	0.23456945	-0.91793442	0.28106518
C	1.69592641	-1.09013017	0.23906386
S	2.54264057	0.36595486	0.91455840
C	1.26221972	1.15518732	-0.02077555
C	-0.05842609	0.49843245	0.21973056
H	-3.31069293	0.11425828	0.14303757
H	-2.75167039	-2.18245487	0.20168939
H	1.44664490	1.89183956	-0.81265117
H	2.16897106	-1.62053067	-0.60210531
O	0.22340187	3.86485124	-0.81915633
H	0.46137203	4.19752446	0.05585924
H	-0.57609258	3.34475707	-0.61052485
O	-4.54753573	1.38903855	-0.21118751
H	-3.74889945	1.95139534	-0.29657454
H	-5.03110029	1.82458117	0.50513481

20
ThiaHX_MeCN_S0-MIN

O	-1.57473878	2.17215391	0.47669193
C	-1.27421905	0.98852728	0.29997160
N	-2.24375041	-0.02487443	0.24911816
C	-1.96931423	-1.36463822	0.05919591
N	-0.79317636	-1.90599729	-0.10494724
C	0.25829761	-0.98556584	-0.07540040
C	1.59487711	-1.31178437	-0.22619205
S	2.59579955	0.10189602	-0.12949752

C	1.25828000	1.15007209	0.11269592
C	0.06828661	0.43927185	0.11997540
H	-3.21948281	0.27025928	0.37164674
H	-2.85691274	-2.00774813	0.05180211
H	1.39088130	2.22493405	0.23725668
H	2.02835647	-2.29944653	-0.38605668
C	-4.27267872	3.85661234	1.00485406
H	-4.77933215	4.47929180	0.25240798
H	-3.18113050	3.91869594	0.87700632
H	-4.55377759	4.20366023	2.01036628
C	-4.65420878	2.45138179	0.83432544
N	-4.92405637	1.30724071	0.69096849
20			
ThiaHX_MeCN_S1-MIN			
O	-1.62504326	2.18371514	0.51006081
C	-1.24774680	1.01785282	0.31860239
N	-2.26453057	-0.04302849	0.26024542
C	-1.99783661	-1.35103160	0.06163835
N	-0.79321885	-1.86089925	-0.11083279
C	0.23121563	-0.93786981	-0.07415846
C	1.59316516	-1.29977471	-0.24023245
S	2.68088290	0.04778481	-0.15077231
C	1.31648338	1.16420628	0.11919320
C	0.06176182	0.48175403	0.13364336
H	-3.23771025	0.26746596	0.38726800
H	-2.86370330	-2.02430692	0.04579517
H	1.49552529	2.23229972	0.24969684
H	1.95673918	-2.31634894	-0.40920673
C	-4.27386663	3.83735369	0.99598413
H	-4.75590373	4.45794727	0.22542758
H	-3.17888061	3.88126185	0.89041285
H	-4.57417990	4.19746080	1.99168349
C	-4.66946722	2.43468404	0.83001919
N	-4.95568465	1.29341529	0.69172196
20			
ThiaHX_MeCN_T1-MIN			
O	-1.62863663	2.18457354	0.50164189
C	-1.26306949	1.00908358	0.31283688
N	-2.25381395	-0.03083549	0.25576647
C	-2.00505855	-1.32633153	0.06212719
N	-0.76838649	-1.85375381	-0.11287426

C	0.21699157	-0.95081909	-0.07474136
C	1.61516928	-1.30873776	-0.23970591
S	2.68815701	0.05062938	-0.14693379
C	1.27453543	1.14649598	0.11805802
C	0.05227201	0.46787288	0.13028654
H	-3.22888584	0.28289895	0.38303509
H	-2.86623064	-2.00021529	0.04526926
H	1.43852701	2.21650021	0.24927088
H	1.97962373	-2.32398347	-0.40522240
C	-4.27429723	3.83967055	1.00036269
H	-4.74983055	4.45121189	0.21922371
H	-3.17893115	3.89720216	0.91087653
H	-4.59335913	4.19794036	1.99043846
C	-4.64491306	2.43029811	0.83207728
N	-4.91186232	1.28424086	0.69439684
20			
ThiaHX_MeCN_T2-MIN			
O	-1.56547727	2.13764442	0.49808508
C	-1.26153161	0.91518281	0.30919629
N	-2.25514968	-0.07373376	0.26933397
C	-1.98361630	-1.38862253	0.07300104
N	-0.76914799	-1.91859372	-0.10750268
C	0.26981956	-1.01544924	-0.08565219
C	1.60858188	-1.31667164	-0.25068696
S	2.64081655	0.12368290	-0.15718241
C	1.28438801	1.16197523	0.10739210
C	0.06198514	0.41955136	0.12304496
H	-3.22612655	0.23681485	0.39986456
H	-2.85007527	-2.05646215	0.06619416
H	1.39834395	2.23660933	0.23805613
H	2.04556395	-2.30086792	-0.42229847
C	-4.30577055	3.90625360	0.99887427
H	-4.79609636	4.50303533	0.21508253
H	-3.21253884	3.99570317	0.90850507
H	-4.63097494	4.26817372	1.98588249
C	-4.65408010	2.49022705	0.84337768
N	-4.90091260	1.33948917	0.71362237
20			
ThiaHX_MeCN_S1/S0			
O	-1.95203638	2.03977119	0.28985852
C	-1.52115980	0.88042358	0.25107139

N	-2.38928762	-0.22836909	0.12244360
C	-1.99860452	-1.53375426	0.01401884
N	-0.71111161	-1.94601282	-0.05212907
C	0.16543729	-0.94923611	0.07121842
C	1.67955317	-1.00855989	-0.14415663
S	2.40857041	0.13641073	1.05922787
C	1.05560170	1.18817508	0.60812655
C	-0.14495440	0.43076777	0.29816537
H	-3.39301106	-0.00901523	0.09407198
H	-2.80017349	-2.27404246	-0.04262852
H	1.14743114	2.27593368	0.54135557
H	1.92653209	-0.65793404	-1.16577290
C	-4.50744581	3.55136048	-0.39651465
H	-5.35010961	4.14681875	-0.77736476
H	-3.63810275	3.67457856	-1.05521381
H	-4.22545246	3.90255894	0.60549680
C	-4.86739323	2.13070653	-0.32879909
N	-5.14100004	0.97956260	-0.27112049
20			
Thio_WAT_S0-MIN			
S	-1.93776489	2.48348571	-0.03753353
C	-1.40577950	0.86970718	-0.01806025
N	-2.28753146	-0.17876171	-0.03449143
C	-1.92246082	-1.51556729	-0.06494580
N	-0.70610666	-1.98066669	-0.06988629
C	0.27267080	-0.99049828	-0.03255981
C	1.63846535	-1.24213267	-0.01972652
S	2.53618398	0.23127414	0.03929139
C	1.12799509	1.21729348	0.03870881
C	-0.02036349	0.43165600	-0.00131029
H	-3.29721087	0.06024365	-0.04853958
H	-2.76839397	-2.21049098	-0.09133473
H	1.20580578	2.30708427	0.08341576
H	2.13154465	-2.21390277	-0.04241450
O	0.84185308	4.45135151	0.22305958
H	0.74144048	4.61169168	-0.72550624
H	-0.02036470	4.05248194	0.42781478
O	-4.84123793	0.98294294	-0.13744416
H	-4.27759157	1.76304597	-0.30434038
H	-5.19850112	1.18330360	0.73986859
20			

Thio_WAT_S1-MIN

S	-1.87138282	2.43137437	0.05104095
C	-1.31259329	0.75329459	0.03016475
N	-2.26168748	-0.26774706	0.01685561
C	-1.88370935	-1.58651588	-0.01763828
N	-0.65928099	-2.04370637	-0.03991335
C	0.33376129	-1.05841437	-0.03074303
C	1.69323669	-1.31540887	-0.05339997
S	2.63330825	0.14466590	-0.03696288
C	1.21783333	1.14642416	-0.00056199
C	0.05220147	0.37260175	0.00130868
H	-3.25116519	-0.00866817	0.02066726
H	-2.71851060	-2.29655722	-0.02444670
H	1.29678617	2.23601279	0.01678519
H	2.16555038	-2.29759315	-0.08122838
O	0.66869596	4.47818790	0.01138668
H	0.05881159	4.42550114	-0.73696713
H	0.06676309	4.45303753	0.76748188
O	-4.73141338	1.18797227	0.01133244
H	-4.82040660	1.78123663	-0.74758804
H	-4.86414629	1.77784377	0.76649166

20

Thio_WAT_S2-MIN

S	-1.99303842	2.49952281	0.03036833
C	-1.37046570	0.90057251	0.01324782
N	-2.31304704	-0.17092522	-0.05194674
C	-1.93792823	-1.45844985	-0.11122121
N	-0.68949360	-1.92854495	-0.10232391
C	0.27676683	-0.96213988	-0.02656925
C	1.66048417	-1.24898934	-0.00190094
S	2.62796230	0.18733045	0.09564568
C	1.17323577	1.19280820	0.09503138
C	-0.00529619	0.46750258	0.03389830
H	-3.31896565	0.06915472	-0.05481084
H	-2.76296319	-2.17899341	-0.17116964
H	1.27386636	2.28124038	0.14422193
H	2.10041231	-2.24885903	-0.03011316
O	0.83835550	4.48728224	0.11278672
H	0.72443624	4.49432814	-0.84760010
H	-0.02436381	4.13677047	0.38813949
O	-4.88703956	0.93500539	-0.09719015

H	-4.36780412	1.73647477	-0.29701355
H	-5.19246174	1.12245071	0.80258528
20			
Thio_WAT_ππ*_La			
S	-1.90639357	2.49562925	0.04691244
C	-1.38164454	0.81889423	0.00926961
N	-2.32436286	-0.21235467	-0.05806286
C	-1.93638604	-1.52845811	-0.11693864
N	-0.70794448	-1.97920774	-0.11209968
C	0.27676776	-0.98672932	-0.04162741
C	1.64573009	-1.22162137	-0.01515149
S	2.58306041	0.26153073	0.07431228
C	1.14752705	1.23349613	0.07025943
C	-0.03088636	0.42689940	0.01135740
H	-3.32512865	0.03399316	-0.05762959
H	-2.76267380	-2.24553408	-0.17462929
H	1.20761580	2.32227552	0.12370671
H	2.13631100	-2.19581335	-0.04187442
O	0.93766009	4.58999098	0.08193857
H	0.92690386	4.54539820	-0.88377012
H	0.07401371	4.20745161	0.29622701
O	-4.94319447	0.94234292	-0.02580695
H	-4.47835982	1.79005128	-0.12235588
H	-5.32596300	1.01530690	0.86002831
20			
Thio_WAT_^{3}nπ*			
S	-1.89131149	2.47750460	-0.08658841
C	-1.37773345	0.81495107	0.06277108
N	-2.31662121	-0.21911064	0.05593568
C	-1.93718004	-1.53187666	0.02127239
N	-0.70517229	-1.98436026	-0.01736527
C	0.27932343	-0.99337907	-0.02373714
C	1.64651346	-1.23202459	-0.06885105
S	2.58357645	0.24785546	-0.06547143
C	1.15823919	1.22922975	-0.00431377
C	-0.02401127	0.42252112	0.01414900
H	-3.31892337	0.02963129	0.06140038
H	-2.76405654	-2.25072081	0.02575133
H	1.22495488	2.31783463	0.03517559
H	2.13231152	-2.20749111	-0.10387879
O	0.94087311	4.60393949	0.10091060

H	0.81959848	4.59141423	-0.85830709
H	0.11169374	4.20131353	0.39755583
O	-4.93028013	0.90922782	-0.06704374
H	-4.49264415	1.73340122	-0.33687624
H	-5.32649810	1.15368060	0.78157649
20			
Thio_WAT_ ππ*_L_b			
S	-1.98571001	2.49214400	-0.01550709
C	-1.39360497	0.89770007	-0.00489103
N	-2.30291163	-0.18608077	-0.02029187
C	-1.96001856	-1.47468903	-0.03732016
N	-0.67373999	-1.94020709	-0.03659169
C	0.24686523	-0.96376606	-0.01770674
C	1.66328436	-1.23460692	-0.01944179
S	2.61650522	0.20092489	0.00080975
C	1.15050119	1.21134379	0.00916347
C	-0.02315606	0.46207804	-0.00269457
H	-3.31683366	0.07130895	-0.02149069
H	-2.77632948	-2.20113789	-0.05499767
H	1.24504122	2.30087089	0.03156731
H	2.10415994	-2.23265121	-0.03491576
O	0.81294107	4.45711282	0.12355841
H	0.70328585	4.57568334	-0.82998259
H	-0.03756681	4.04299493	0.34823244
O	-4.82201784	0.95062830	-0.06886102
H	-4.26985656	1.74094989	-0.23981030
H	-5.16818628	1.14294073	0.81523703
20			
Thio_WAT_S2/S1			
S	-1.97537536	2.50876768	0.05794835
C	-1.35668714	0.89041862	-0.00277949
N	-2.31581605	-0.17507397	-0.07433608
C	-1.94544913	-1.46485026	-0.11654464
N	-0.69630404	-1.93476670	-0.09437953
C	0.27573500	-0.97399146	-0.02656892
C	1.65477226	-1.25438779	0.00236973
S	2.61085892	0.19599053	0.08183786
C	1.17740226	1.20342241	0.07750410
C	-0.00751584	0.46250203	0.01673860
H	-3.32076223	0.08087593	-0.07179060
H	-2.76796427	-2.18622522	-0.17253370

H	1.27411839	2.29102942	0.11888127
H	2.10417933	-2.24787317	-0.01151207
O	0.83714603	4.53503041	0.03417737
H	0.65858983	4.38953488	-0.90480108
H	0.01485878	4.19468065	0.41908058
O	-4.89118385	0.93925864	-0.03502229
H	-4.40666952	1.75208701	-0.26685509
H	-5.11128113	1.10711206	0.89265103

20
Thio_WAT_S1/S0

S	-1.95289380	2.37415600	-0.29074720
C	-1.25253170	0.75534660	0.36429000
N	-2.21465860	-0.27925660	0.32716100
C	-1.84427180	-1.58726570	0.30517180
N	-0.64118630	-2.05234480	0.08895810
C	0.32880960	-1.07101000	-0.13829790
C	1.63936080	-1.32962200	-0.49027260
S	2.55567360	0.12245280	-0.77073950
C	1.17007330	1.11632910	-0.42398270
C	0.05972150	0.36108600	-0.09019200
H	-3.18062380	-0.04774460	0.58226150
H	-2.66115930	-2.29448650	0.46041740
H	1.25082620	2.20594150	-0.45042660
H	2.08299770	-2.31614350	-0.62094530
O	0.34915830	4.15319970	0.27237090
H	-0.35129840	4.78540980	0.10024020
H	0.01154630	3.70235520	1.03663650
O	-4.25187220	1.63714590	0.01675260
H	-4.62994170	1.70598980	-0.87345940
H	-4.65507740	2.37200300	0.51886880

20
Thio_MeCN_S0-MIN

S	-1.10851660	2.70392764	0.55329316
C	-0.95159483	1.04652400	0.29894013
N	-2.02534175	0.18439090	0.27422141
C	-1.93962412	-1.18678727	0.09204150
N	-0.84762177	-1.87301219	-0.09275570
C	0.30687576	-1.09251733	-0.09886069
C	1.59150052	-1.59298925	-0.28349141
S	2.75884183	-0.32870562	-0.22996709

C	1.58162578	0.89005171	0.03869571
C	0.30535043	0.34482606	0.08600270
H	-2.96134759	0.58379106	0.41060155
H	-2.90682469	-1.70007329	0.11761195
H	1.85439961	1.93941800	0.15106480
H	1.87980957	-2.63173893	-0.44369168
C	-4.76741061	3.89523544	1.04530863
H	-5.34990317	4.40276686	0.26247708
H	-3.71538956	4.21492428	0.99238067
H	-5.18349073	4.14871700	2.03135541
C	-4.80952849	2.44404071	0.84280520
N	-4.81380958	1.27115324	0.67815565
20			
Thio_MeCN_S1-MIN			
S	-0.64457010	2.62084150	0.58316775
C	-0.59406982	0.87630288	0.29079358
N	-1.78624386	0.15514260	0.29419626
C	-1.80248315	-1.19750186	0.06632430
N	-0.76449493	-1.95885011	-0.17073031
C	0.46232594	-1.28934267	-0.18198700
C	1.68424345	-1.89543610	-0.40746311
S	3.00244137	-0.76080493	-0.34342976
C	1.92891927	0.56498196	-0.00833515
C	0.59632034	0.14642933	0.04993624
H	-2.66393508	0.65272756	0.46405074
H	-2.80071234	-1.64839316	0.09451078
H	2.32516354	1.57251038	0.12775406
H	1.85677976	-2.95297781	-0.60739140
C	-5.61863009	4.18920674	1.14709146
H	-6.29599753	4.29302082	0.28653202
H	-5.01813073	5.10576361	1.24544591
H	-6.21431212	4.04880285	2.06121175
C	-4.73349078	3.03575630	0.94747522
N	-4.02112300	2.10576257	0.78703582
20			
Thio_MeCN_S2-MIN			
S	-1.14508198	2.72200931	0.61085547
C	-0.88737679	1.05334534	0.28198434
N	-2.04560183	0.20016716	0.17239215
C	-1.95892496	-1.11558170	-0.04202054
N	-0.82729007	-1.82073042	-0.20717992

C	0.31802445	-1.07959669	-0.13748341
C	1.61204098	-1.61963574	-0.28399587
S	2.85019006	-0.40287030	-0.12699074
C	1.64867282	0.84908453	0.14028333
C	0.33398066	0.36430618	0.10737105
H	-2.97510595	0.62992133	0.28355134
H	-2.91291322	-1.65349185	-0.08286618
H	1.95313947	1.88284994	0.31112174
H	1.84887319	-2.66726924	-0.47341886
C	-4.82949020	3.87706614	1.14398276
H	-5.39968901	4.44045937	0.39081088
H	-3.78571008	4.22671619	1.15763157
H	-5.28434037	4.02860123	2.13389344
C	-4.82377367	2.45054068	0.80828494
N	-4.79162332	1.29805102	0.53798164
20			
Thio_MeCN_ππ*_L_a			
S	-1.10497593	2.46556803	1.17934500
C	-0.94575649	0.89191734	0.45950905
N	-2.05191569	0.17009157	-0.00409804
C	-1.92792848	-1.06479597	-0.57678675
N	-0.80655075	-1.72584950	-0.76367285
C	0.32747300	-1.05681191	-0.31660290
C	1.63786833	-1.55585215	-0.40419227
S	2.83985415	-0.44912756	0.26003082
C	1.59726907	0.70559356	0.66414425
C	0.29007855	0.23868235	0.29288158
H	-2.98625386	0.58477557	0.08257769
H	-2.87105814	-1.51801112	-0.89949116
H	1.82713895	1.65720980	1.14315229
H	1.93082973	-2.51953507	-0.82364975
C	-4.82207520	3.93836314	1.26076042
H	-5.41841025	4.60422837	0.62001426
H	-3.78570520	4.30467083	1.31283889
H	-5.25368115	3.92637589	2.27232393
C	-4.80803919	2.58129636	0.70598463
N	-4.77016132	1.48515291	0.26112008
20			
Thio_MeCN_^{3}nπ			
S	-0.60938832	2.46011027	1.12793383
C	-0.57351927	0.84303095	0.44105751

N	-1.77258305	0.23400127	0.06747685
C	-1.79793441	-1.02494378	-0.46917710
N	-0.76472996	-1.79922576	-0.69420262
C	0.46594068	-1.24362401	-0.33516875
C	1.68515669	-1.88112289	-0.48064571
S	3.01310049	-0.90485173	0.07193984
C	1.94833457	0.39672357	0.51629987
C	0.61245277	0.08877035	0.24564370
H	-2.65042545	0.74560896	0.19359686
H	-2.79923916	-1.38793546	-0.72269071
H	2.35063737	1.31235313	0.95197058
H	1.84810820	-2.87871292	-0.88828463
C	-5.64852625	4.16093533	1.23400682
H	-6.37053039	4.32441562	0.42143130
H	-5.06939468	5.08192729	1.38758603
H	-6.19347091	3.92454388	2.15888682
C	-4.74820835	3.05311510	0.88829311
N	-4.02778037	2.15882331	0.61023548
20			
Thio_MeCN_ ππ*_L_b			
S	-1.18136121	2.47230914	1.30011813
C	-0.89927384	0.94958527	0.52083926
N	-2.02524195	0.21103047	0.06429550
C	-1.94246381	-0.99227743	-0.52231736
N	-0.79994623	-1.66721069	-0.75171909
C	0.32741575	-1.02979869	-0.32800282
C	1.62140759	-1.56777882	-0.46383055
S	2.82960135	-0.52826423	0.17885011
C	1.63429582	0.67091067	0.65253245
C	0.34353530	0.28883714	0.33314063
H	-2.95481488	0.63481140	0.18293404
H	-2.88987679	-1.44353939	-0.83183236
H	1.94617852	1.59145138	1.14721325
H	1.86480115	-2.52956105	-0.91739728
C	-4.84849147	3.90377714	1.20435539
H	-5.41718990	4.55453843	0.52412074
H	-3.81239259	4.26593890	1.28557449
H	-5.31843555	3.91764367	2.19854112
C	-4.81665746	2.53347679	0.68437282
N	-4.76308965	1.42806235	0.26440067
20			

Thio_MeCN_S2/S1

S	-1.12644041	2.56694535	1.34706336
C	-0.85120090	1.10712635	0.54211044
N	-2.03668683	0.42616555	-0.03559201
C	-1.97033649	-0.75052362	-0.66000644
N	-0.85234633	-1.48239775	-0.86386247
C	0.28907633	-0.91971058	-0.38026385
C	1.56085394	-1.54047988	-0.50805824
S	2.83893511	-0.58412772	0.21577443
C	1.65134172	0.63622731	0.69350729
C	0.32048657	0.36096808	0.31944021
H	-2.94649199	0.89212106	0.06368986
H	-2.92191913	-1.14572542	-1.03415879
H	1.97074029	1.52392462	1.24380507
H	1.74623865	-2.50839960	-0.97876830
C	-4.78230246	3.61549715	1.38801645
H	-5.10796578	4.46104013	0.76442252
H	-3.72777409	3.73909717	1.68371153
H	-5.42193261	3.55305982	2.27996521
C	-4.86133849	2.36612478	0.62580678
N	-4.87293695	1.34700966	0.01958602

20

Thio_MeCN_S1/S0

S	-0.63685862	2.65234776	0.73066325
C	-0.63009874	0.74523637	0.86961648
N	-1.87616719	0.15544370	0.56668874
C	-1.91551975	-1.15785979	0.14570216
N	-0.93266367	-1.86304657	-0.26724651
C	0.32001247	-1.23279219	-0.25610799
C	1.46467667	-1.75973931	-0.75395051
S	2.81493462	-0.64583636	-0.61692872
C	1.79167387	0.56288206	0.12858480
C	0.48971426	0.11805205	0.26670624
H	-2.65391204	0.44821932	1.11981726
H	-2.90596677	-1.59687823	0.15139502
H	2.21280130	1.50060423	0.45284452
H	1.58236646	-2.72082621	-1.22522907
C	-5.50149258	3.92054401	0.90376313
H	-5.99084540	3.66798209	-0.03474755
H	-5.46665103	5.00237107	1.01545117
H	-6.05646513	3.48817337	1.73380683

C	-4.13414844	3.39264807	0.89995239
N	-3.07739010	2.98641700	0.89540748

S5 Supporting references

1 C. Reichardt, C. Wen, R. A. Vogt and C. E. Crespo-Hernández, *Photochem. Photobiol. Sci.*, 2013, **12**, 1341–1350.
2 C. Reichardt, R. A. Vogt and C. E. Crespo-Hernández, *J. Chem. Phys.*, 2009, **131**, 0–15.
3 M. M. Brister and C. E. Crespo-Hernández, *J. Phys. Chem. Lett.*, 2019, **10**, 2156–2161.
4 J. J. Snellenburg, S. P. Laptenok, R. Seger, K. M. Mullen and I. H. M. van Stokkum, *J. Stat. Softw.*, 2012, **49**, 1–22.
5 Y. Yagci, S. Jockusch and N. J. Turro, *Macromolecules*, 2007, **40**, 4481–4485.
6 R. Schmidt, C. Tanielian, R. Dunsbach and C. Wolff, *J. Photochem. Photobiol. A Chem.*, 1994, **79**, 11–17.
7 Y. Liu, S. Pujals, P. J. M. Stals, T. Paulöhrl, S. I. Presolski, E. W. Meijer, L. Albertazzi and A. R. A. Palmans, *J. Am. Chem. Soc.*, 2018, **140**, 3423–3433.
8 N. Faruqui, A. Bella, J. Ravi, S. Ray, B. Lamarre and M. G. Ryadnov, *J. Am. Chem. Soc.*, 2014, **136**, 7889–7898.
9 Q. Miao, L.-L. Bi, X. Li, S. Miao, J. Zhang, S. Zhang, Q. Yang, Y.-H. Xie, J. Zhang and S.-W. Wang, *Int. J. Mol. Sci.*, 2013, **14**, 1370–1382.
10 F. Benyettou, T. Prakasam, A. R. Nair, I.-I. Witzel, M. Alhashimi, T. Skorjanc, J.-C. Olsen, K. C. Sadler and A. Trabolsi, *Chem. Sci.*, 2019, **10**, 5884–5892.
11 B. Smolková, M. Lunova, A. Lynnyk, M. Uzhytchak, O. Churpita, M. Jirsa, S. Kubinova, O. Lunov and A. Dejneka, *Cell. Physiol. Biochem*, 2019, **52**, 119–140.
12 H. Wang and J. A. Joseph, *Free Radic. Biol. Med.*, 1999, **27**, 612–616.
13 K. Andersson, P. A. Malmqvist, B. O. Roos, A. J. Sadlej and K. Wolinski, *J. Phys. Chem.*, 1990, **94**, 5483–5488.
14 K. Andersson, P.-Å. Malmqvist and B. O. Roos, *J. Chem. Phys.*, 1992, **96**, 1218–1226.
15 I. Fdez. Galván, M. Vacher, A. Alavi, C. Angeli, F. Aquilante, J. Autschbach, J. J. Bao, S. I. Bokarev, N. A. Bogdanov, R. K. Carlson and others, *J. Chem. Theory Comput.*, 2019, **15**, 5925–5964.
16 F. Aquilante, J. Autschbach, A. Baiardi, S. Battaglia, V. A. Borin, L. F. Chibotaru, I. Conti, L. De Vico, M. Delcey, I. Fdez. Galván and others, *J. Chem. Phys.*, 2020, **152**, 214117.
17 T. H. Dunning Jr, *J. Chem. Phys.*, 1989, **90**, 1007–1023.
18 S. Miertuš, E. Scrocco and J. Tomasi, *Chem. Phys.*, 1981, **55**, 117–129.
19 F. Aquilante, R. Lindh and T. Bondo Pedersen, *J. Chem. Phys.*, 2007, **127**, 114107.
20 G. Ghigo, B. O. Roos and P.-Å. Malmqvist, *Chem. Phys. Lett.*, 2004, **396**, 142–149.
21 N. Forsberg and P.-Å. Malmqvist, *Chem. Phys. Lett.*, 1997, **274**, 196–204.
22 I. Fdez. Galván, M. G. Delcey, T. B. Pedersen, F. Aquilante and R. Lindh, *J. Chem. Theory Comput.*, 2016, **12**, 3636–3653.
23 M. Sholokh, R. Improta, M. Mori, R. Sharma, C. Kenfack, D. Shin, K. Voltz, R. H. Stote, O.A. Zaporoshets, M. Botta and Y. Tor, *Angew. Chem. Int. Ed.*, 2016, **55**, 7974–7978.